Supporting Information for

Phenothiazine-based covalent organic frameworks with low exciton binding energies for photocatalysis

Weitao Wang,[a#] Haotian Wang,[a#] Xiaohui Tang,[a] Jinlei Huo,[a] Yan Su,[a] Chuangye Lu,[a] Yujian Zhang,*[c] Hong Xu*[b] and Cheng Gu*[a,d]

[a]State Key Laboratory of Luminescent Materials and Devices, Institute of Polymer Optoelectronic Materials and Devices, South China University of Technology, No. 381 Wushan Road, Tianhe District, Guangzhou 510640, P. R. China

[b]Institute of Nuclear and New Energy Technology, Tsinghua University, Beijing, 100084, P. R. China

[c]Department of Chemistry, Zhejiang Normal University, Jinhua 321004, P. R. China

[d]Guangdong Provincial Key Laboratory of Luminescence from Molecular Aggregates, South China University of Technology, No. 381 Wushan Road, Tianhe District, Guangzhou, 510640, P. R. China

Table of Contents

Supplementary Materials and Methods

Materials and methods.

Materials.

10-Methyl-phenothiazine-3,7-dicarbaldehyde (MPTz, 98%, Jilin Chinese Academy of Sciences-Yanshen Technology Co., Ltd.), 1,3,5-tris(4-aminophenyl)benzene (TAPB, 98%, Jilin Chinese Academy of Sciences-Yanshen Technology Co., Ltd.), (benzene-1,3,5-triyl)triacetonitrile (BTTA, 98%, Jilin Chinese Academy of Sciences-Yanshen Technology Co., Ltd.), 1,3,6,8-tetrakis(4-aminophenyl)pyrene (TAPP, 98%, Jilin Chinese Academy of Sciences-Yanshen Technology Co., Ltd.), 1,4-dioxane (99.7%, Shanghai Macklin Biochemical Co., Ltd), mesitylene (98+%, Alfa Aesar), 1-butanol (*n*-BuOH, 99+%, Acros Organics), 1,2-dichlorobenzene (*o*-DCB, 99%, TCI), acetic acid (AcOH, AR, Shanghai Richjoint Chemical Reagents Co., Ltd.), potassium hydroxide (KOH, 97%, Energy Chemical), hydrogen peroxide (H_2O_2, 30% w/w, Guangzhou Chemical Reagent Factory), *n*-hexane (99.5%, Energy Chemical), acetone (AR, Guangzhou Chemical Reagent Factory), tetrahydrofuran (THF, 99.5%, Energy Chemical), dichloromethane (DCM, 99.9%, Energy Chemical), acetonitrile (ACN, 99.9%, Energy Chemical), methanol (MeOH, 99.9%, Energy Chemical), *N*,*N*-dimethylformamide (DMF, 99.5%, Energy Chemical), *N*,*N*-dimethylacetamide (DMA, 99.5%, Energy Chemical), methyl methacrylate (MMA, 99%, Energy Chemical), ethyl α-bromophenylacetate (EBP, 97%, Energy Chemical).

N_2 (99.9999%) was purchased from MULAI Company (China).

Synthesis of PTz-TPB-COF: A 10-mL pyrex tube was charged with MPTz (15.35 mg, 0.057 mmol), TAPB (13.36 mg, 0.038 mmol), 1,4-dioxane (0.2 mL), mesitylene (0.8 mL) and aqueous acetic acid (0.1 mL, 6 M). This mixture was sonicated for ten minutes, degassed through three freeze-pump-thaw cycles, sealed under vacuum, and heated at 120 ºC for three days. The reaction mixture was cooled to room temperature and the precipitate was centrifuged and washed with THF for several times, then further treated using Soxhlet extraction with THF. The solvent was removed under vacuum at 80 ºC to afford the corresponding product as brown powder in an isolated yield of 82%.

Synthesis of PTz-BTA-COF: A 10-mL pyrex tube was charged with MPTz (15.35 mg, 0.057 mmol), BTTA (7.42 mg, 0.038 mmol), *n*-BuOH (1 mL) and aqueous KOH solution (0.1 mL, 4 M). This mixture was sonicated for ten minutes, degassed through three freeze-pump-thaw

cycles, sealed under vacuum, and heated at 120 ºC for three days. The reaction mixture was cooled to room temperature and the precipitate was centrifuged and washed with H_2O and THF for several times, then further treated using Soxhlet extraction with THF. The solvent was removed under vacuum at 80 ºC to afford the corresponding product as red powder in an isolated yield of 67%.

Synthesis of PTz-Py-COF: A 10-mL pyrex tube was charged with MPTz (15.08 mg, 0.056 mmol), TAPP (15.87 mg, 0.028 mmol), *o*-DCB (0.7 mL), *n*-BuOH (0.3 mL) and aqueous acetic acid (0.1 mL, 6 M). This mixture was sonicated for ten minutes, degassed through three freeze-pump-thaw cycles, sealed under vacuum, and heated at 120 ºC for three days. The reaction mixture was cooled to room temperature and the precipitate was centrifuged and washed with THF for several times, then further treated using Soxhlet extraction with THF. The solvent was removed under vacuum at 80 ºC to afford the corresponding product as orange powder in an isolated yield of 76%.

Synthesis of OPTz-BTA-COF: PTz-BTA-COF (60 mg) was suspended in AcOH (20 mL) and H_2O_2 aqueous solution (30% w/w, 1 mL) was then added. The mixture was stirred at 80 ºC for 4 h and then cooled to room temperature. Afterwards, the precipitate was centrifuged and washed with saturated $NaHCO_3$ solution, H_2O, acetone and MeOH for several times, then further treated using Soxhlet extraction with acetone, THF and MeOH. The solvent was removed under vacuum at 80 ºC to afford the corresponding product as yellow powder in an isolated yield of 90%.

Methods.

General instrumental analysis.

Solid-state ^{13}C cross polarization magic angle spinning nuclear magnetic resonance spectra (^{13}C CPMAS NMR) were recorded on a JEOL JNM-ECA600 MHz, 3.2 mm rotor, MAS of 20 kHz, recycle delay of 1 sec. Fourier-transform infrared (FT-IR) spectra were recorded on an IFS 66V/S Fourier transform infrared spectrophotometer. UV-vis-NIR spectra were recorded on a Shimadzu UV-3600 spectrometer. Photoluminescence spectra were recorded on a Shimadzu RF-5301PC spectrofluorophotometer. Temperature-dependent photoluminescence spectra were recorded on a HORIBA Fluorolog-3 module fluorescence spectrometer. PL quantum yields were recorded on a Hamamarsu C11347-11 Quantaurus-QY. The photoluminescence decay profiles were measured by using time-correlated single photon

counting (TCSPC) mode with a picosecond light source. DPV was performed with a Shanghai Chenhua Instruments electrochemical analyzer CHI760E C18477 with a $Ag/AgNO_3$ (0.01 M in ACN) reference electrode using ACN as the solvent. Elemental analysis was performed on an Elementar Vario EL elemental analyser. TG measurements were performed on a Rigaku Thermo plus EVO2 under N_2, by heating to 900 °C at a rate of 5 °C min^{-1}. Field-emission scanning electron microscopy (FE-SEM) was performed on a Hitachi Regulus 8100 operating at an accelerating voltage of 5.0 kV. High-resolution transmission electron microscopy (HR-TEM) images were obtained on a JEOL model JEM-3200 and a TEM JEOL 2100F with an acceleration voltage of 300 kV. PXRD data were recorded on a Rigaku model RINT Ultima III diffractometer by depositing powder on glass substrate, from $2\theta = 1°$ to 40° with 0.01° increment.

Computational calculations.

The crystalline structures of the COFs were determined using the density-functional tight-binding (DFTB).[S1] The calculations were carried out with the DFTB+ program package version 17.1.[S2] DFTB[S1] is an approximate density functional theory method based on the tight-binding approach and utilizes an optimized minimal LCAO Slater-type all-valence basis set in combination with a two-center approximation for Hamiltonian matrix elements. The Coulombic interaction between partial atomic charges was determined using the self-consistent charge (SCC) formalism. Lennard-Jones-type dispersion was employed in all calculations to describe van der Waals and possible π-stacking interactions The lattice dimensions were optimized simultaneously with the geometry. Standard DFTB parameters for X–Y element pair (X, Y = C, H, O, N and S) interactions were employed from the 3ob set.[S3–S6]

The powder X-ray diffraction (PXRD) pattern simulation was performed using a software package for crystal determination from PXRD pattern, implemented in Reflex module of Materials Studio. We performed Pawley refinement to optimize the lattice parameters iteratively until the R_P and R_{WP} values converge. The pseudo-Voigt profile function was used for whole profile fitting and Berar-Baldinozzi function[S7] was used for asymmetry correction during the refinement processes. All simulation works were performed using the computing resources at National Supercomputing Center in Shenzhen.

Gas sorption measurements.

N_2 sorption measurements were performed on BELSORP-mini (Bel Japan, Inc.) automated volumetric sorption analysers. The desired temperature of 77 K were controlled by liquid nitrogen bath. Before measurement, the samples were degassed in vacuum at 120 °C for 11 h. By using the non-local density functional theory (NLDFT) model, the pore sizes were derived from the N_2 sorption curve.

Exciton binding energy (E_b):

The E_b was measured by temperature-dependent photoluminescence technology, from which the E_b can be estimated from the integral emission intensity by fitted with equation (1):

$$I(T) = \frac{I_0}{1 + Ae^{-E_B/k_BT}} \quad (1)$$

where I_0 is the integral intensity at 0 K, E_B is the E_b, and k_B is the Boltzmann constant.

Gel permeation chromatography (GPC) measurements.

The number-(M_n) and weight-(M_w) average molecular weights and dispersity (Đ = M_w/M_n) of the polymers were estimated by a Waters e2695 gel permeation chromatography system. DMF/LiBr solution (0.05 M LiBr) was used as eluent at a flow rate of 1 mL min^{-1}. A set of monodispersed polymethylmethacrylate (PMMA), covering the M_w range of 10^3–10^7 g mol^{-1}, were utilized as standards for molecular weight calibration.

Photocatalytic polymerization experiments

A 5-mL vial was charged with a small stir bar and photocatalyst and transferred into an argon-atmosphere glovebox. Solvent (DMA, 1 mL), monomer (MMA, 1 mL, 9.35 mmol), and initiator (EBP) were then added sequentially via pipette. The amount of EBP used was 16.9 μL (93.5 μmol), except for entry 4 (33.8 μL) and entry 6 (8.45 μL). The vial was then sealed, placed inside a darkroom (315 × 300 × 450 mm) illuminated by Xe light (300 W, 300-1600 nm), and stirred for given hours. Afterwards, the photocatalyst (for entry 2-8) was centrifuged and washed with THF for several times, meanwhile the supernate was collected and vacuumed at 40 ºC to removed THF. The remanent liquid or the reaction (for entry 1) was poured into 200 mL MeOH and stirred overnight. The resulting precipitate was then isolated by vacuum filtration and washed with excess MeOH. The product was dried under vacuum to reveal a white powder. The product was re-dissolved in DMF for analysis of M_w and M_n by GPC.

Supporting Figures

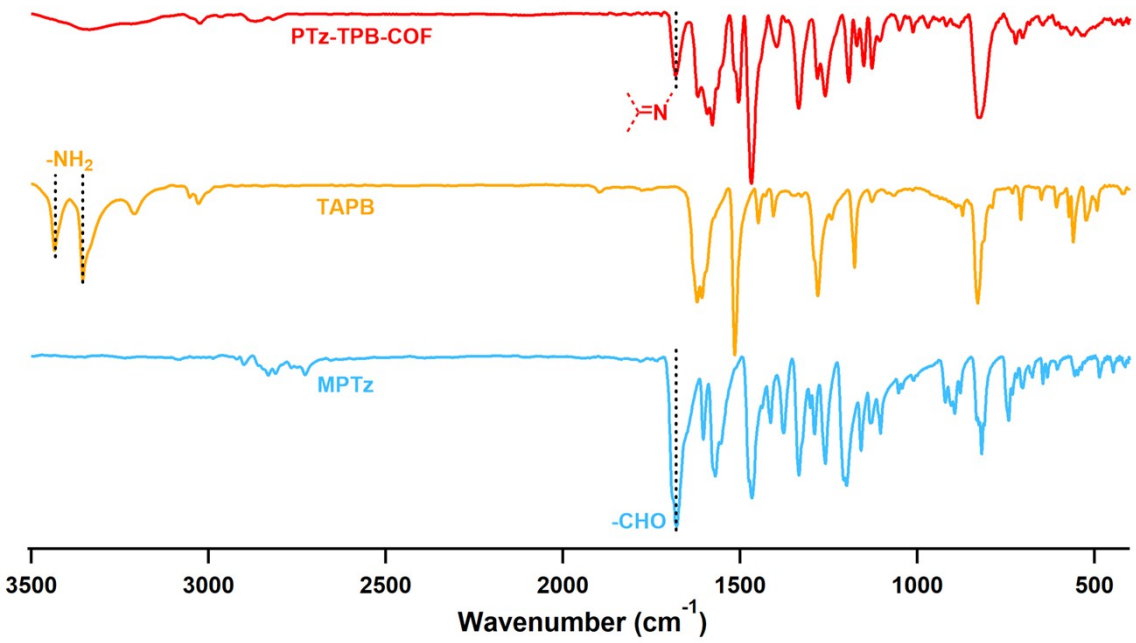

Figure S1. FT-IR spectra of the monomers and PTz-TPB-COF.

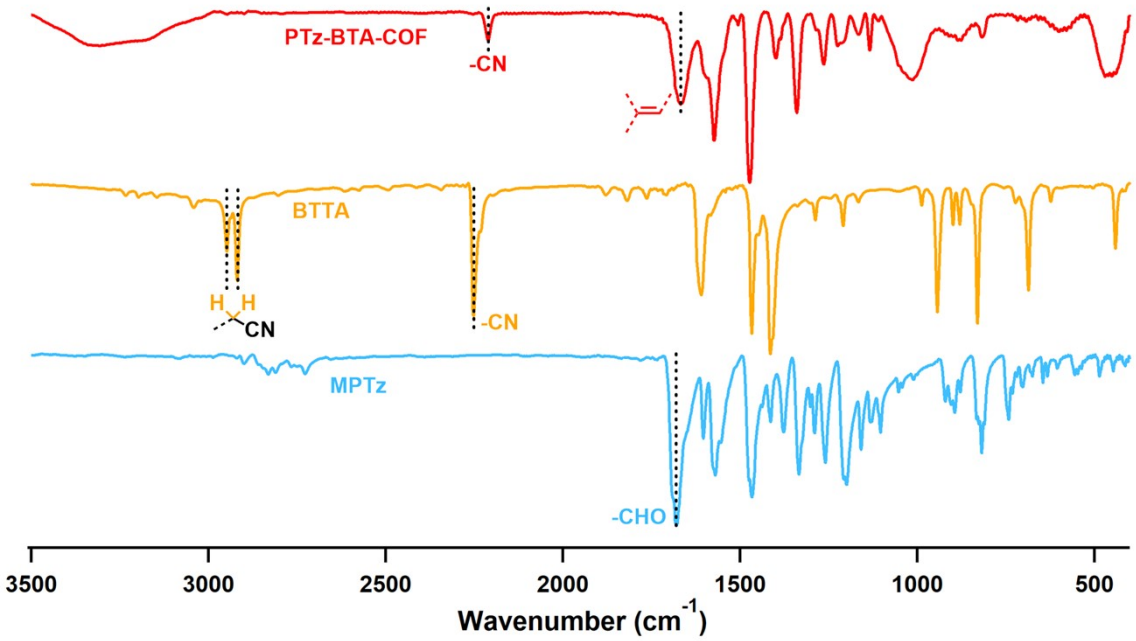

Figure S2. FT-IR spectra of the monomers and PTz-BTA-COF.

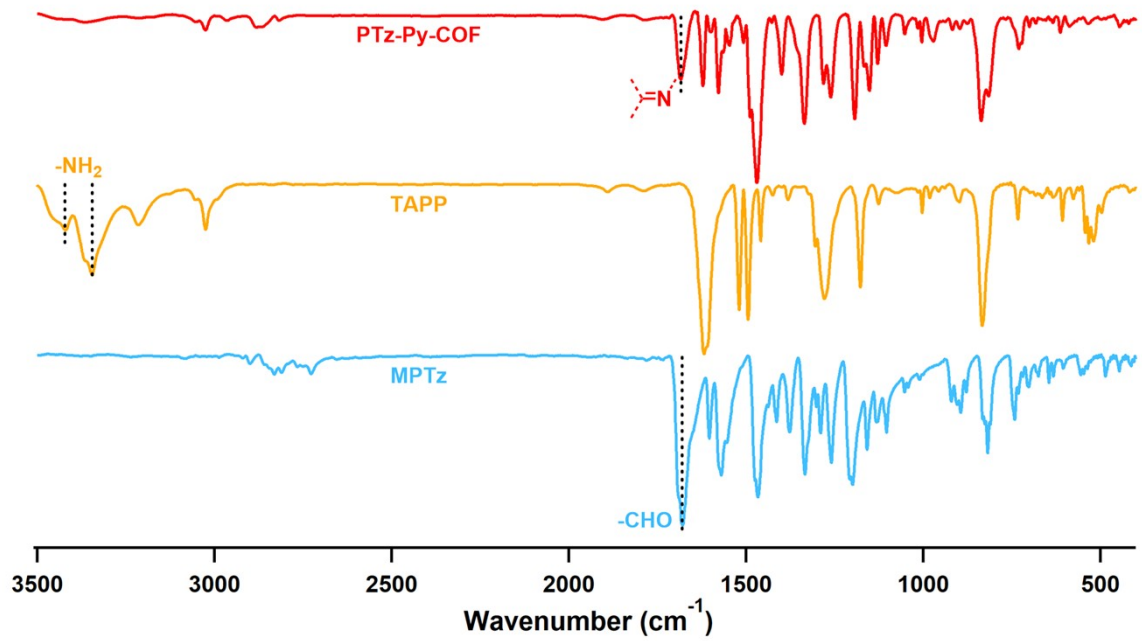

Figure S3. FT-IR spectra of the monomers and PTz-Py-COF.

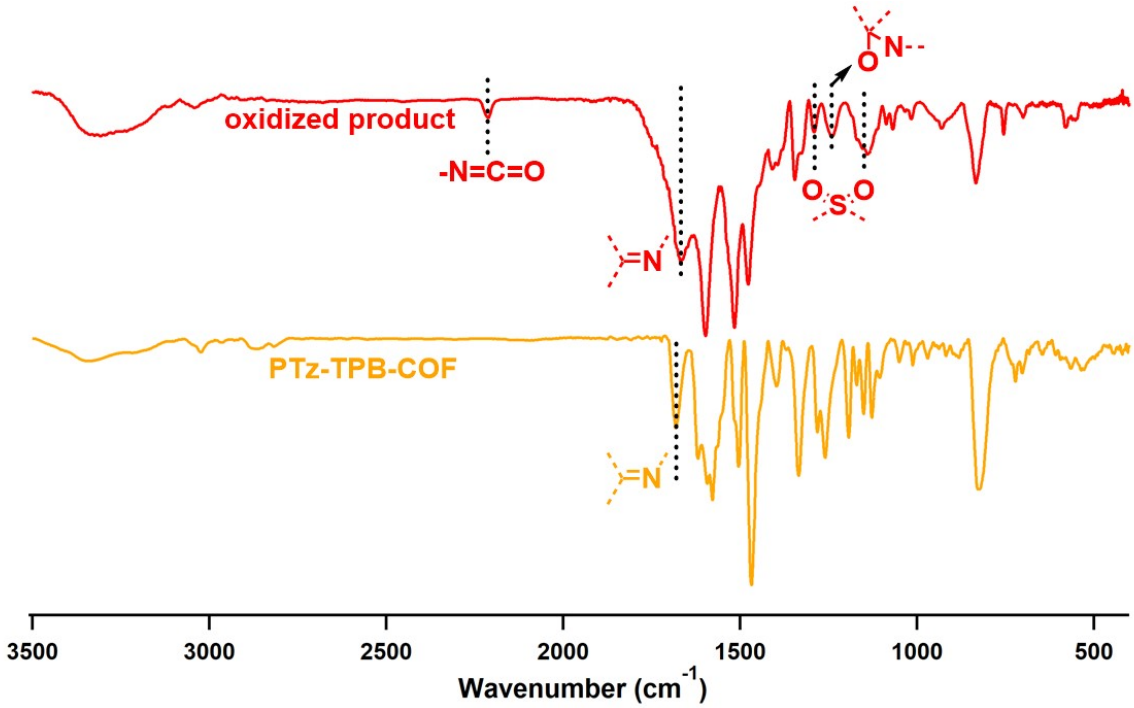

Figure S4. FT-IR spectra of PTz-TPB-COF and its oxidized product.

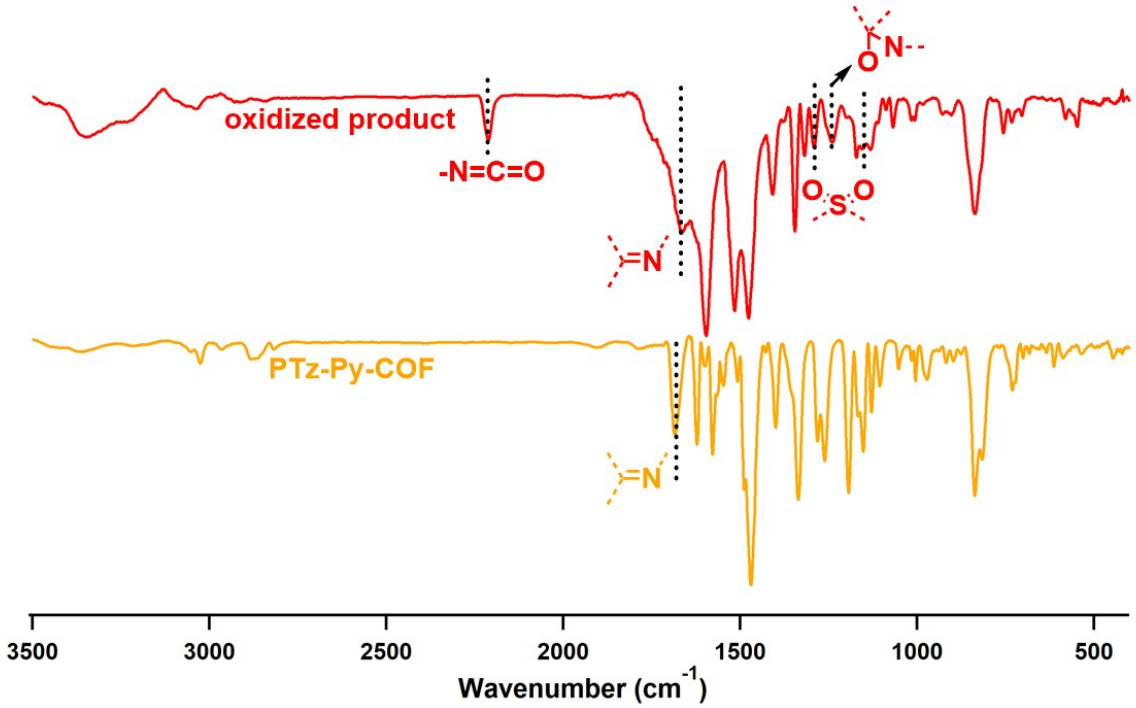

Figure S5. FT-IR spectra of PTz-Py-COF and its oxidized product.

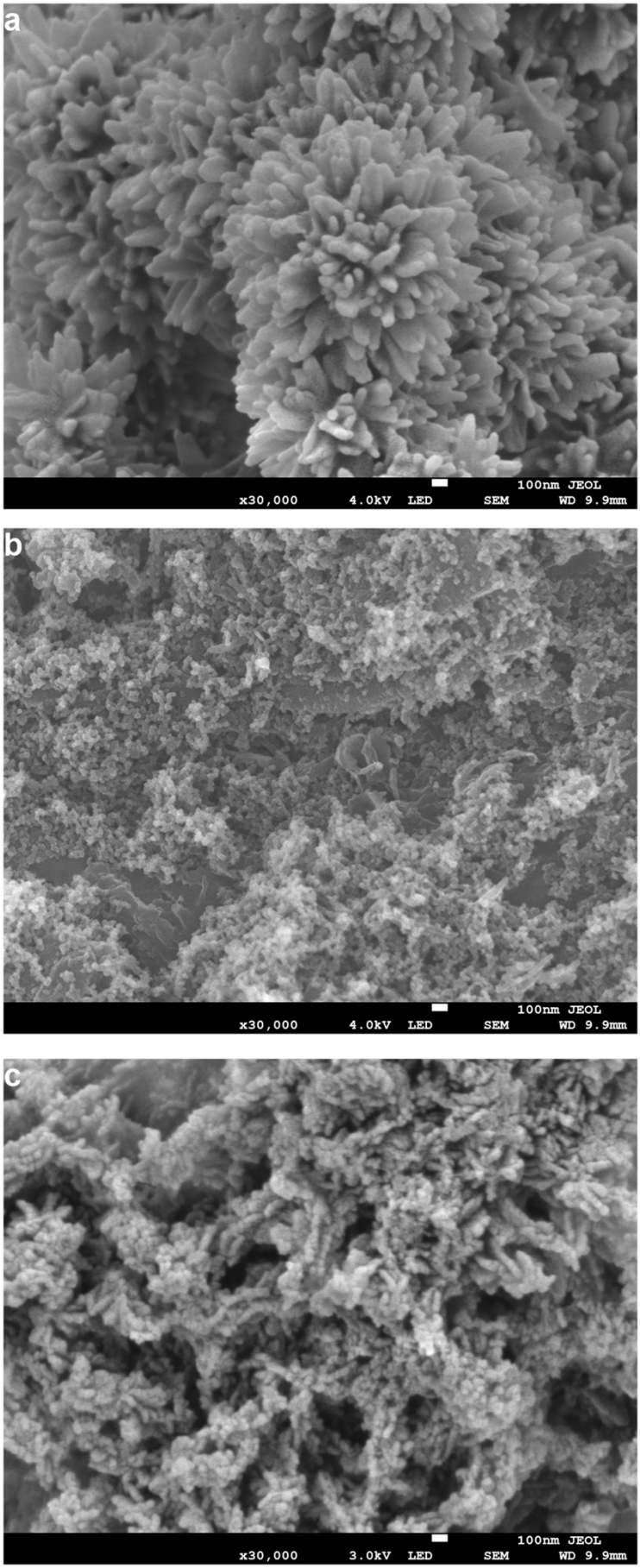

Figure S6. SEM images of (a) PTz-TPB-COF, (b) PTz-BTA-COF, and (c) PTz-Py-COF.

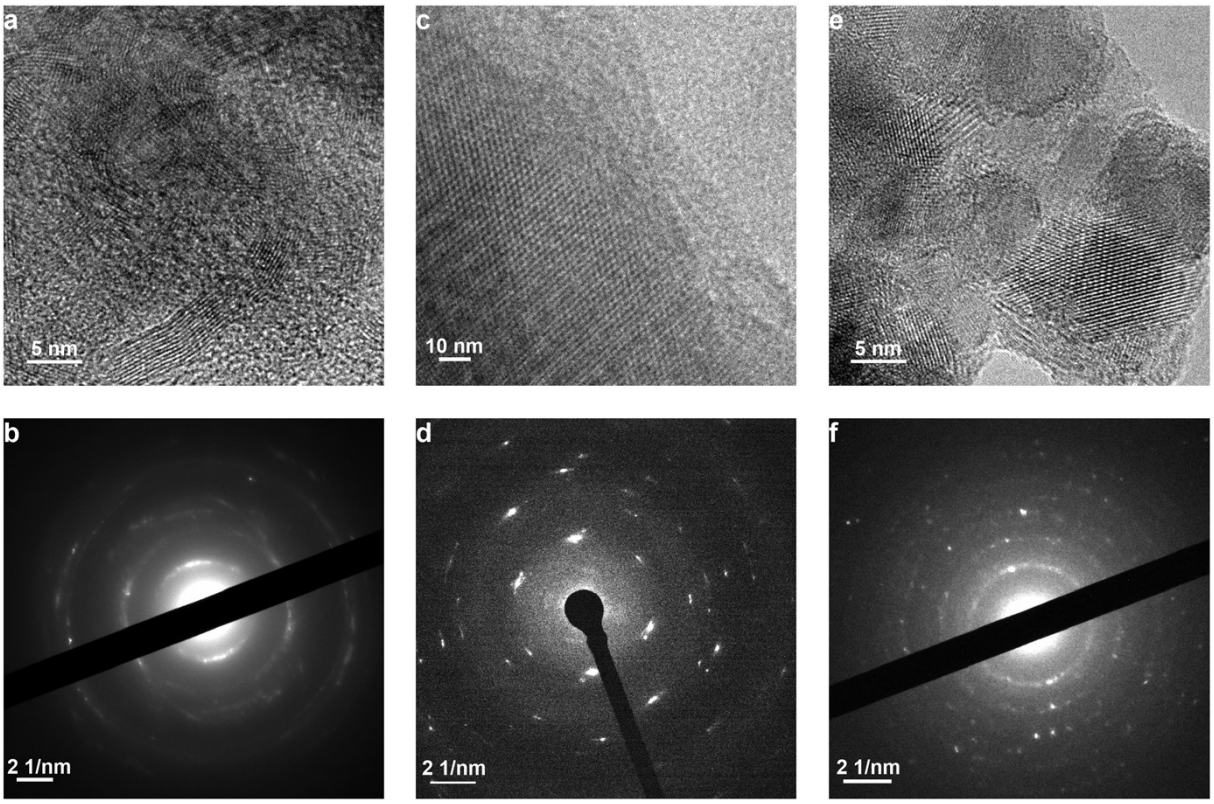

Figure S7. (a) High-resolution TEM image and (b) SAED patterns for PTz-TPB-COF. (c) High-resolution TEM image and (d) SAED patterns for PTz-BTA-COF. (e) High-resolution TEM image and (f) SAED patterns for PTz-Py-COF.

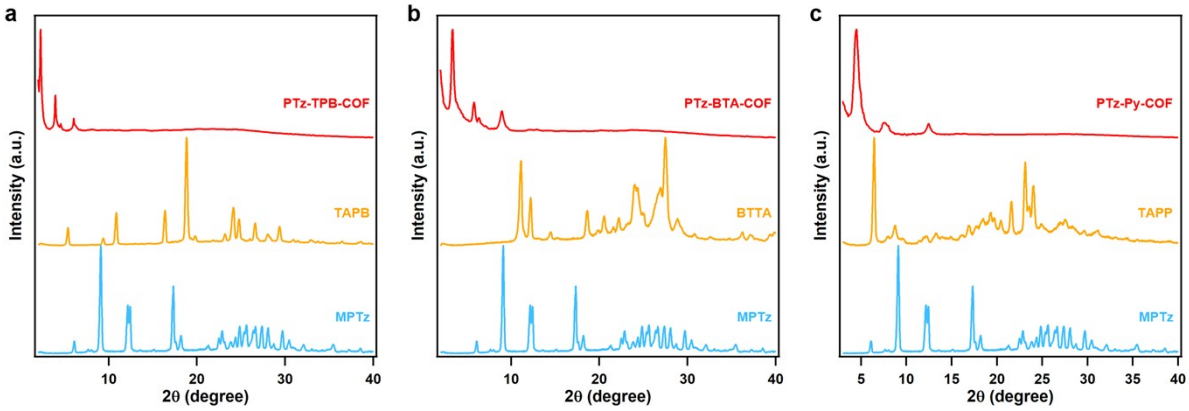

Figure S8. PXRD patterns of (a) PTz-TPB-COF, (b) PTz-BTA-COF, and (c) PTz-Py-COF in comparasion with their monomers.

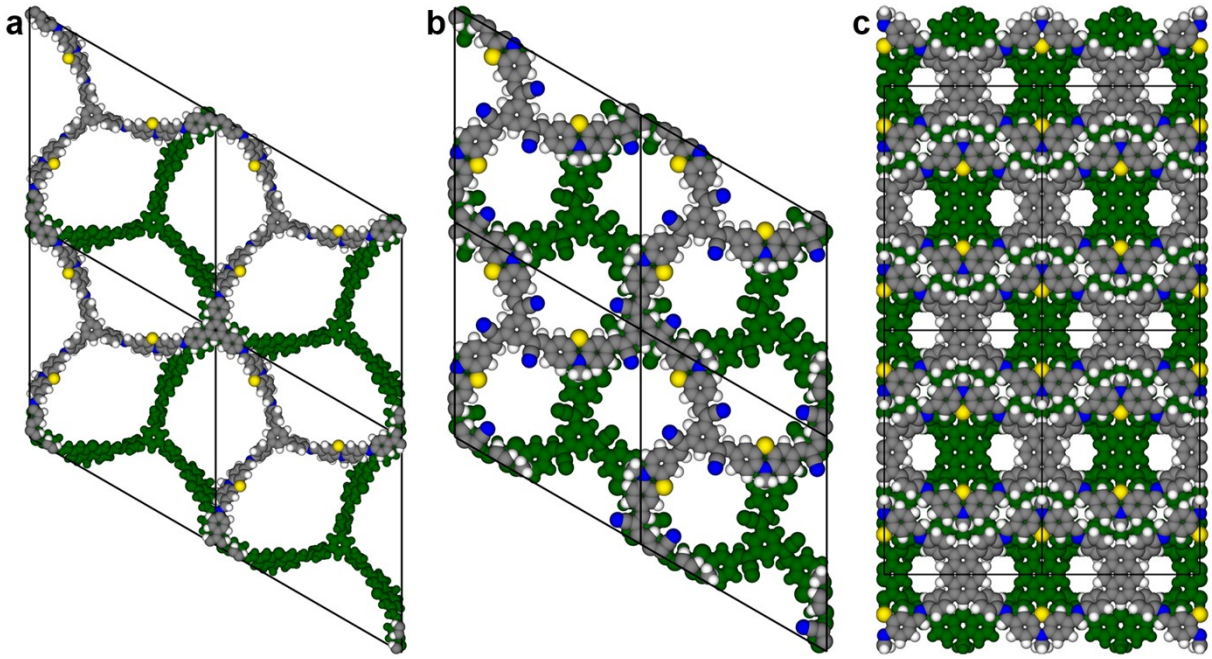

Figure S9. Simulated AB stacking modes for (a) PTz-TPB-COF, (b) PTz-BTA-COF, and (c) PTz-Py-COF.

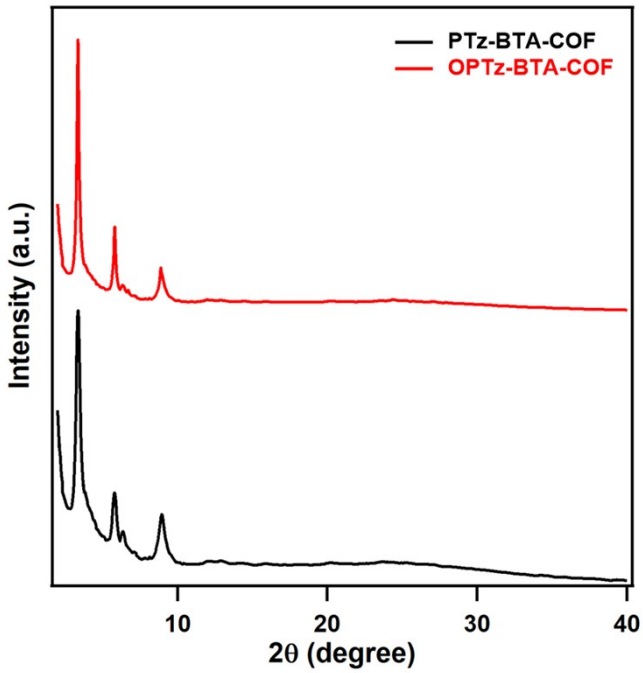

Figure S10. PXRD patterns of PTz-BTA-COF and OPTz-BTA-COF.

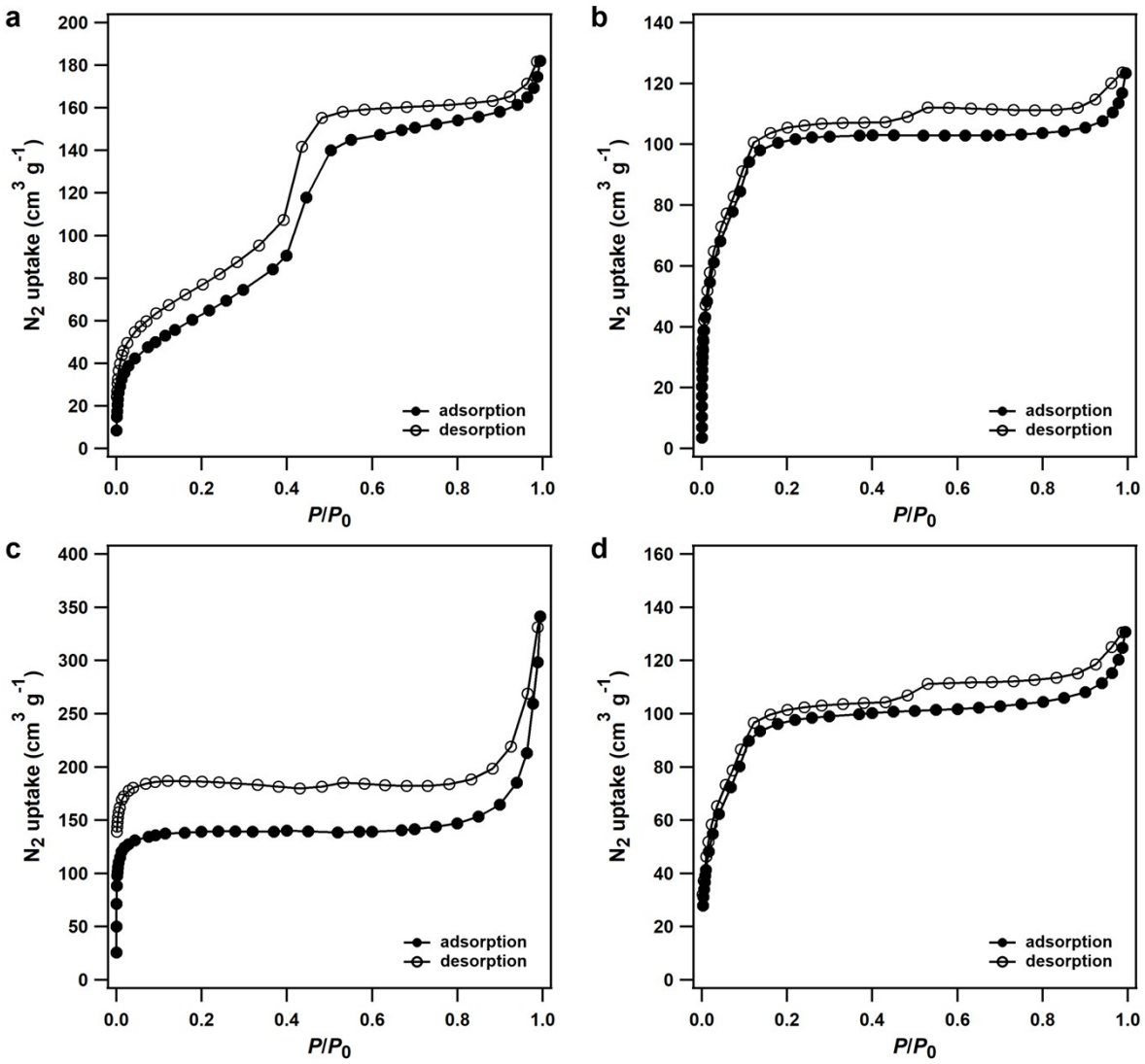

Figure S11. N_2-sorption profiles of (a) PTz-TPB-COF, (b) PTz-BTA-COF, (c) PTz-Py-COF, and (d) OPTz-BTA-COF at 77 K.

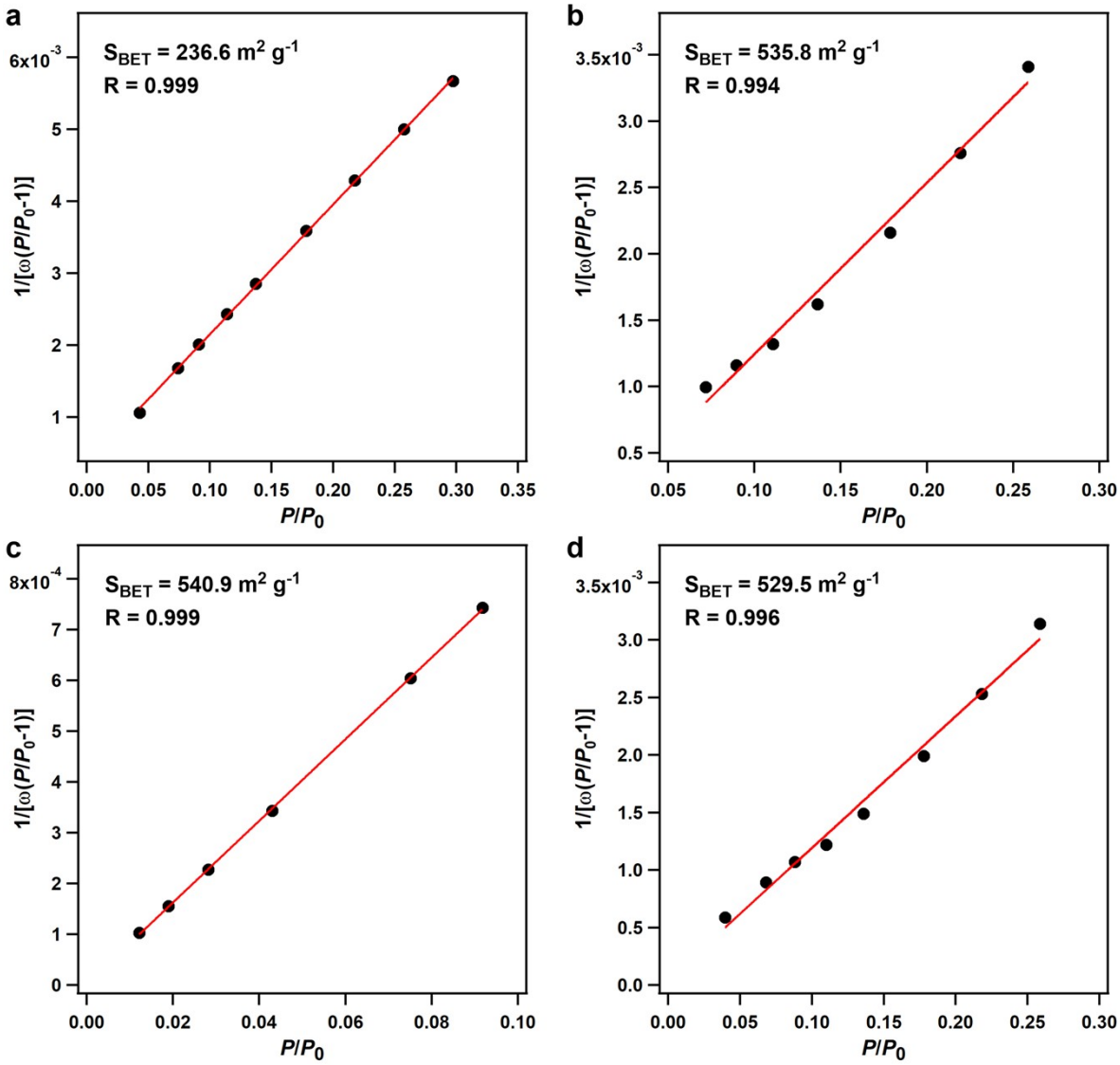

Figure S12. BET plots for (a) PTz-TPB-COF, (b) PTz-BTA-COF, (c) PTz-Py-COF, and (d) OPTz-BTA-COF.

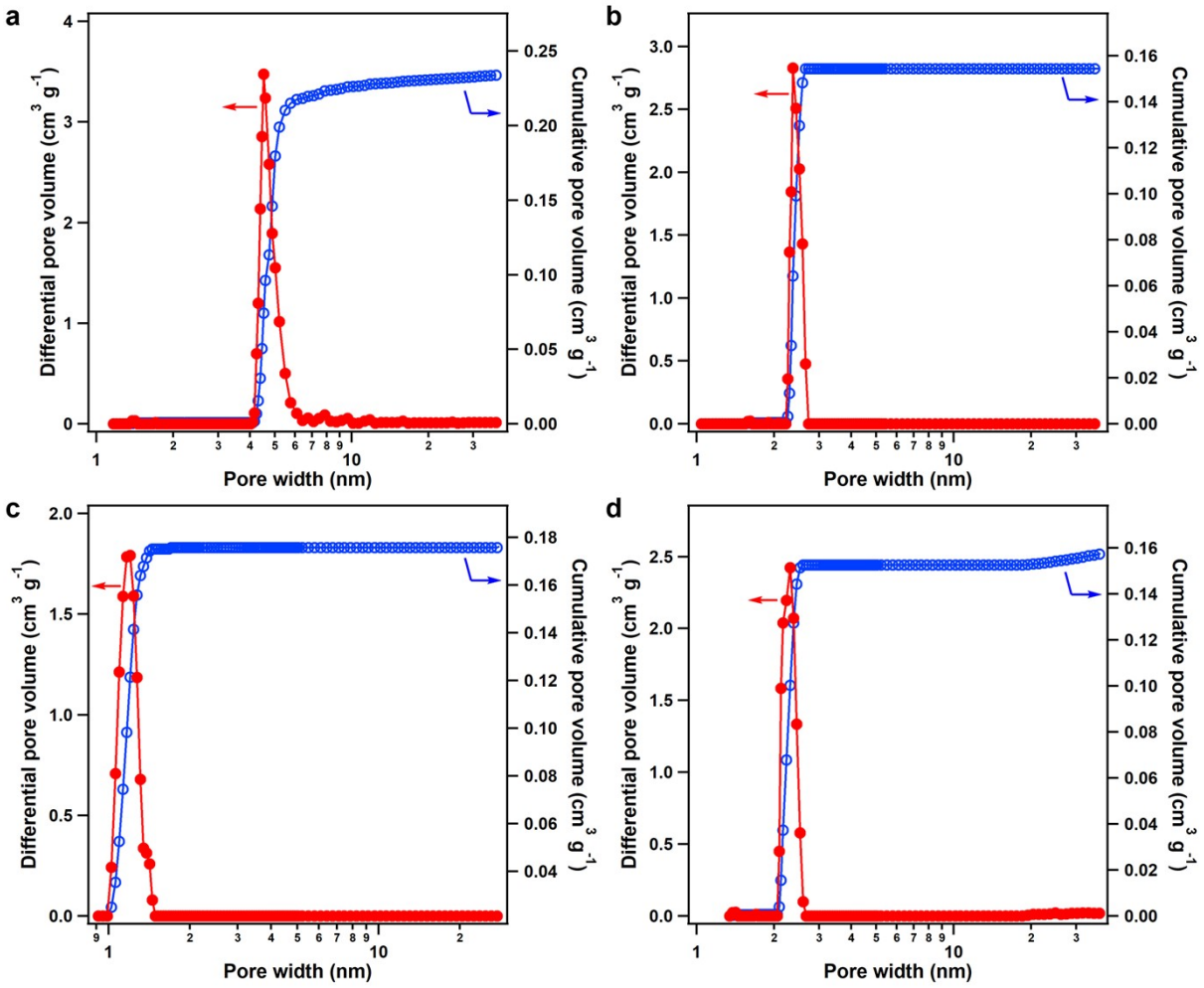

Figure S13. Pore volume and pore-size distribution profiles for (a) PTz-TPB-COF, (b) PTz-BTA-COF, (c) PTz-Py-COF, and (d) OPTz-BTA-COF.

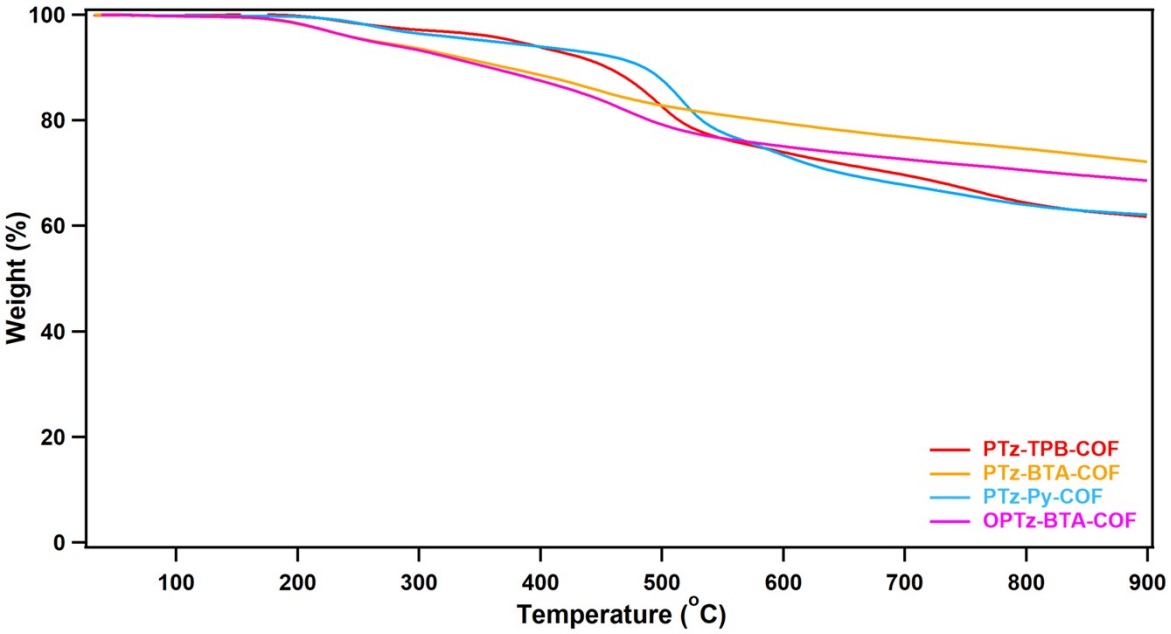

Figure S14. TG curves of PTz-TPB-COF, PTz-BTA-COF, PTz-Py-COF, and OPTz-BTA-COF.

In the temperature range of 200 to 300 ºC, PTz-TPB-COF, PTz-BTA-COF, PTz-Py-COF, and OPTz-BTA-COF showed the weight loss of 2.8, 4.3, 3.5, and 4.3 wt%, which were very close to the weight percentages of the $-CH_3$ groups in every COF (3.2, 4.1, 2.9, and 4.0 wt% for PTz-TPB-COF, PTz-BTA-COF, PTz-Py-COF, and OPTz-BTA-COF). Therefore, the weight loss before 300 ºC was because of the removal of the $-CH_3$ groups from the COF skeletons. Moreover, for PTz-BTA-COF and OPTz-BTA-COF, the continuous weight loss (13.1 and 13.8 wt%) from 300 to 500 ºC was because of the removal of −CN groups (14.3 and 14.2 wt%) from its skeleton.

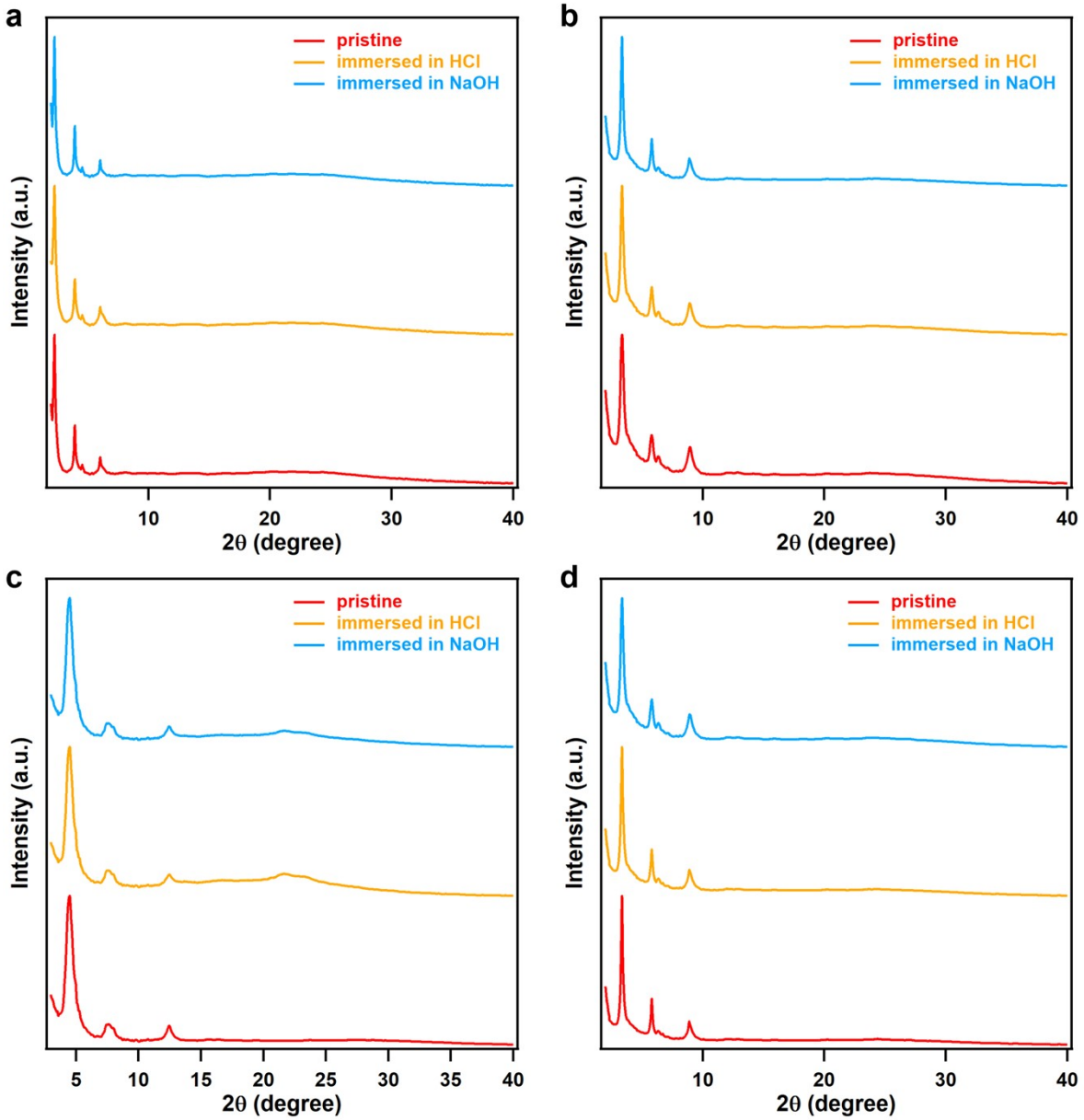

Figure S15. PXRD patterns of (a) PTz-TPB-COF, (b) PTz-BTA-COF, (c) PTz-Py-COF, and (d) OPTz-BTA-COF before and after immersion into concentrated HCl or NaOH solutions at room temperature for 3 d.

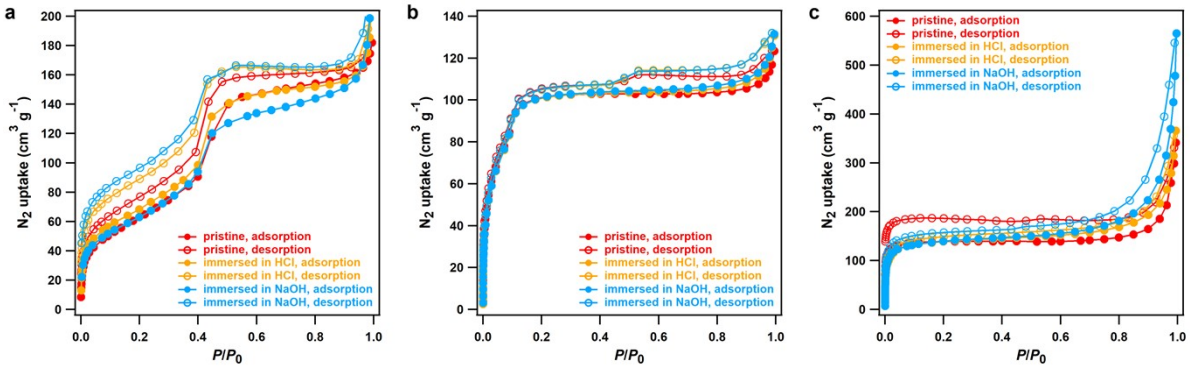

Figure S16. N_2-sorption profiles of (a) PTz-TPB-COF, (b) PTz-BTA-COF, and (c) PTz-Py-COF before and after immersion into concentrated HCl or NaOH solutions at room temperature for 3 d.

PTz-TPB-COF, PTz-BTA-COF, and PTz-Py-COF upon treated with HCl exhibited the BET surface areas of 245.3, 532.1, and 538.4 $m^2\ g^{-1}$, whereas they showed the BET surface areas of 250.7, 533.1, and 537.9 $m^2\ g^{-1}$ upon base treatments.

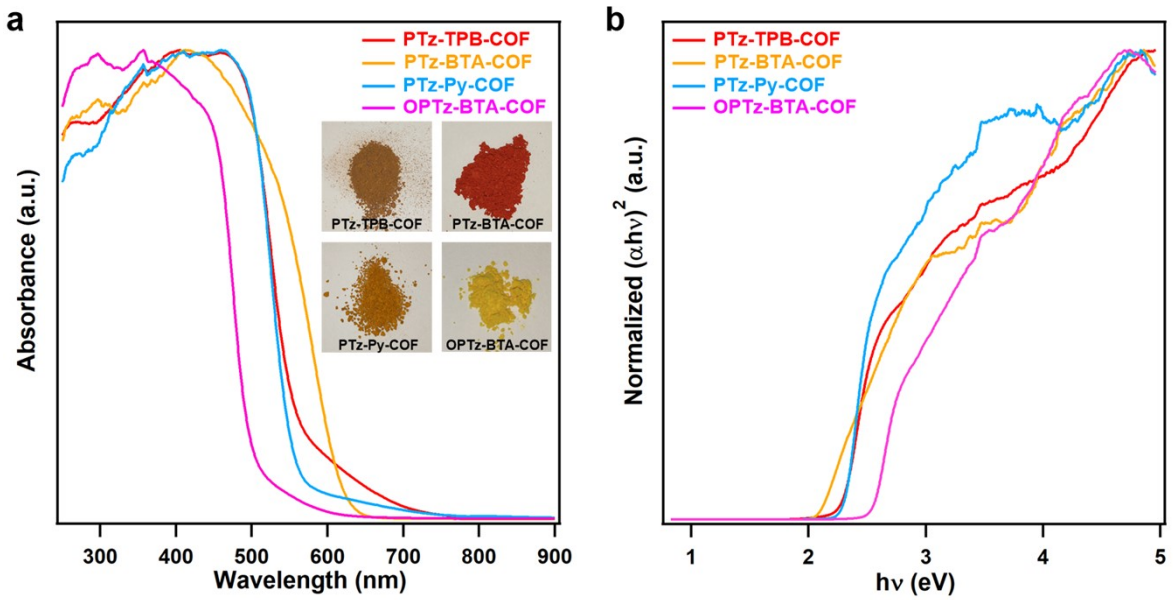

Figure S17. (a) UV-vis diffuse reflectance spectra of PTz-TPB-COF, PTz-BTA-COF, PTz-Py-COF, and OPTz-BTA-COF. The insets are the photos of PTz-TPB-COF, PTz-BTA-COF, PTz-Py-COF, and OPTz-BTA-COF under sunlight. (b) Tauc plots of PTz-TPB-COF, PTz-BTA-COF, PTz-Py-COF, and OPTz-BTA-COF.

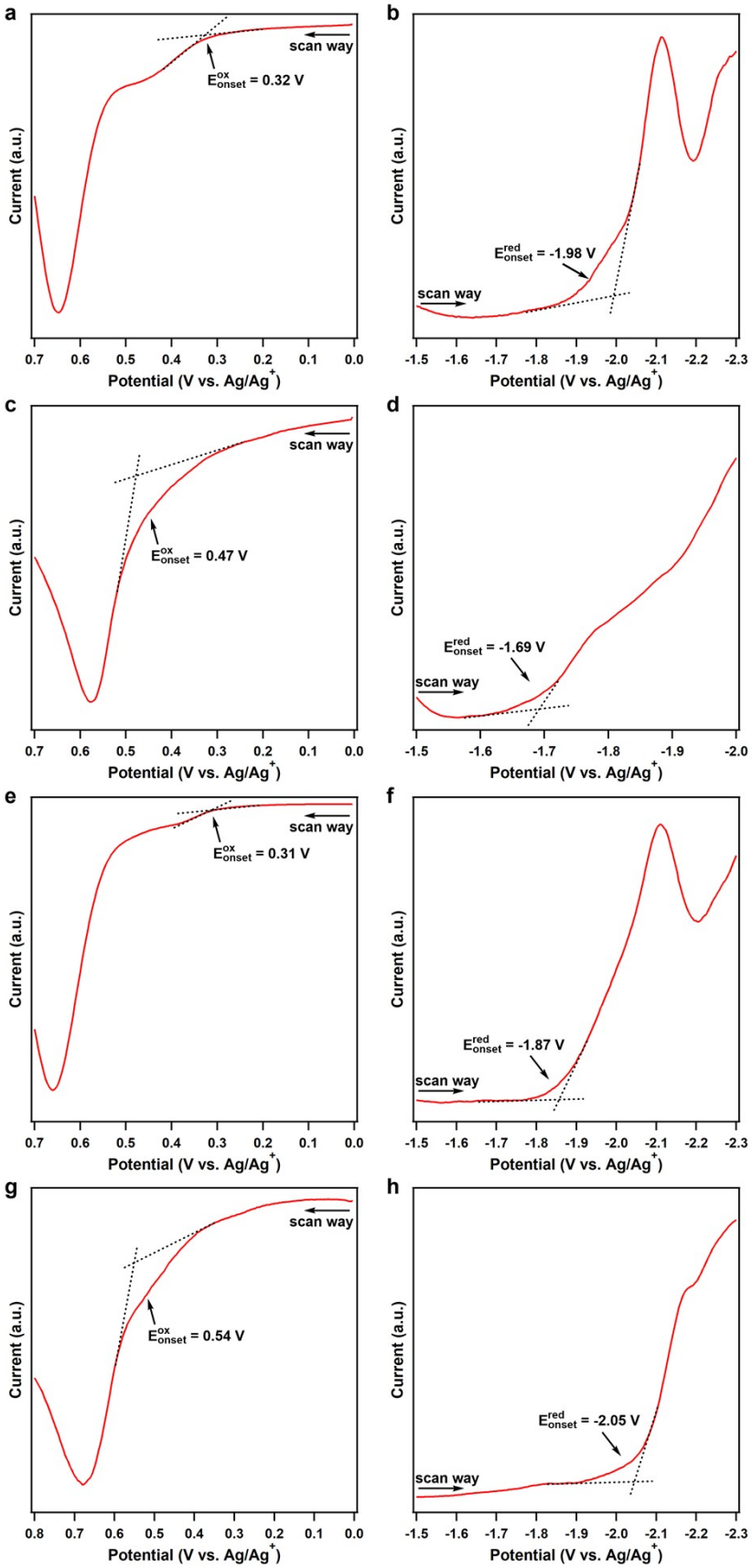

Figure S18. (a) Positive and (b) negative DPV profiles of PTz-TPB-COF. (c) Positive and (d) negative DPV profiles of PTz-BTA-COF. (e) Positive and (f) negative DPV profiles of PTz-Py-COF. (g) Positive and (h) negative DPV profiles of OPTz-BTA-COF.

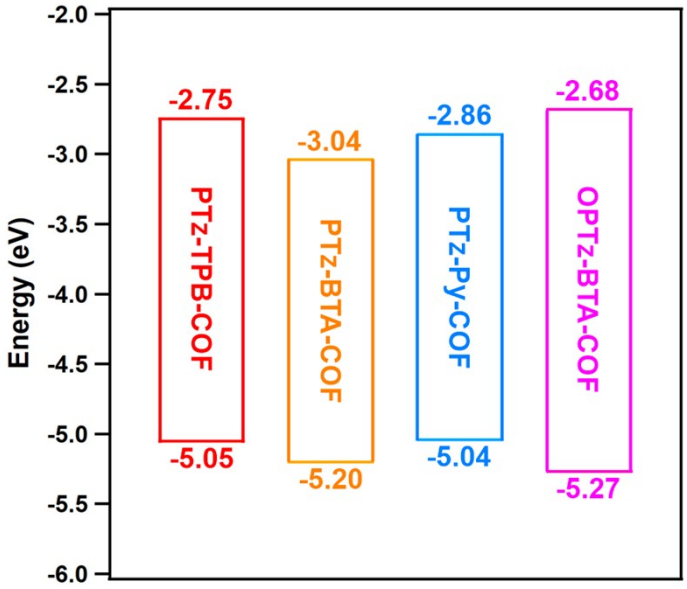

Figure S19. Electrochemical bandgaps of PTz-TPB-COF, PTz-BTA-COF, PTz-Py-COF, and OPTz-BTA-COF.

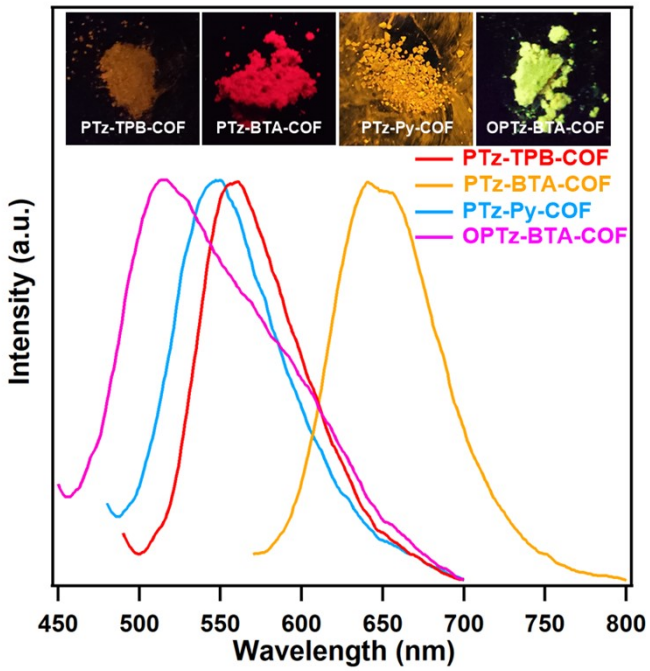

Figure S20. Photoluminescence spectra of PTz-TPB-COF, PTz-BTA-COF, PTz-Py-COF, and OPTz-BTA-COF powders in air. The insets are the photos of PTz-TPB-COF, PTz-BTA-COF, PTz-Py-COF, and OPTz-BTA-COF under 365-nm UV light.

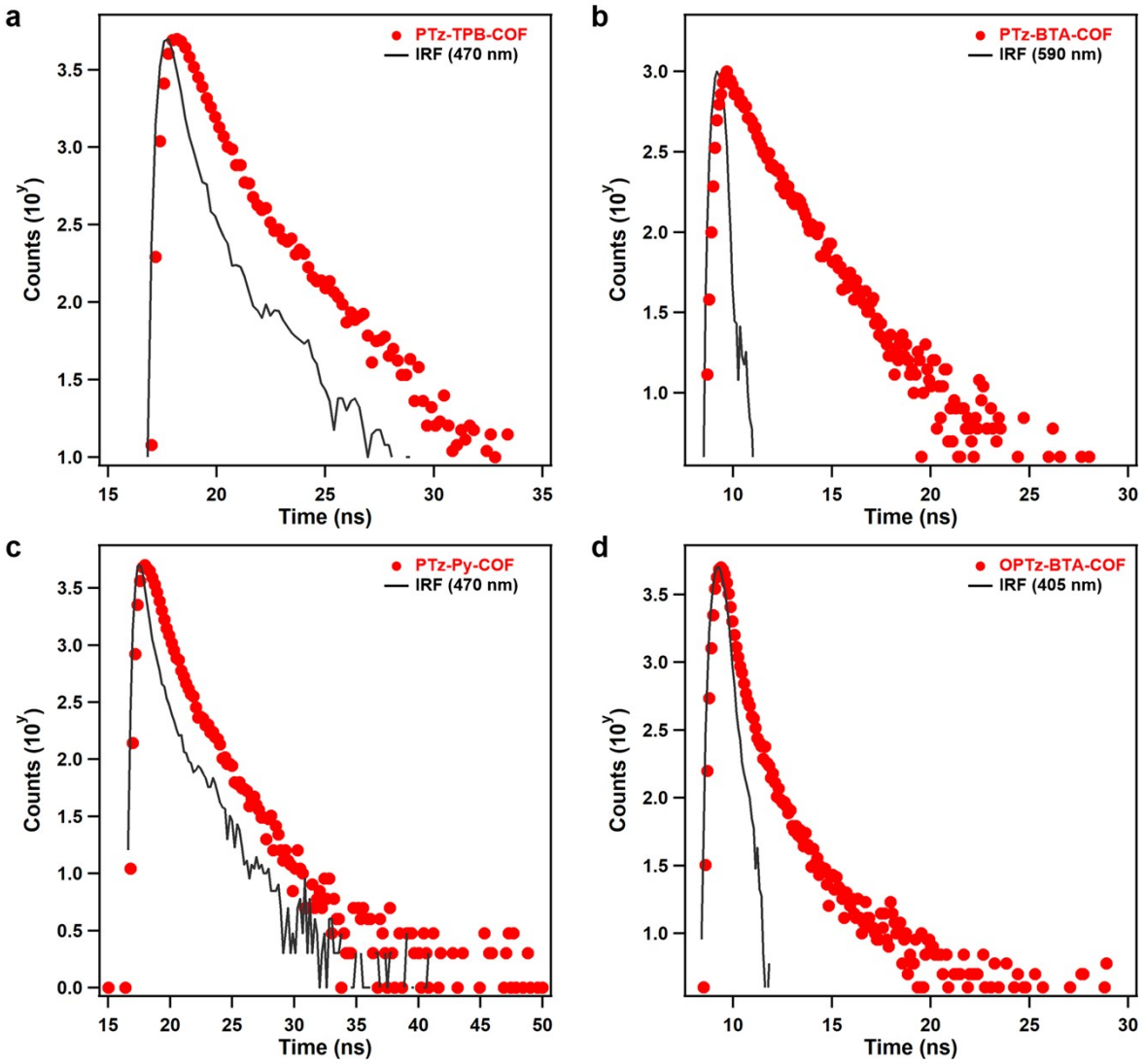

Figure S21. Photoluminescence decay profiles of (a) PTz-TPB-COF, (b) PTz-BTA-COF, (c) PTz-Py-COF, and (d) OPTz-BTA-COF powders in air.

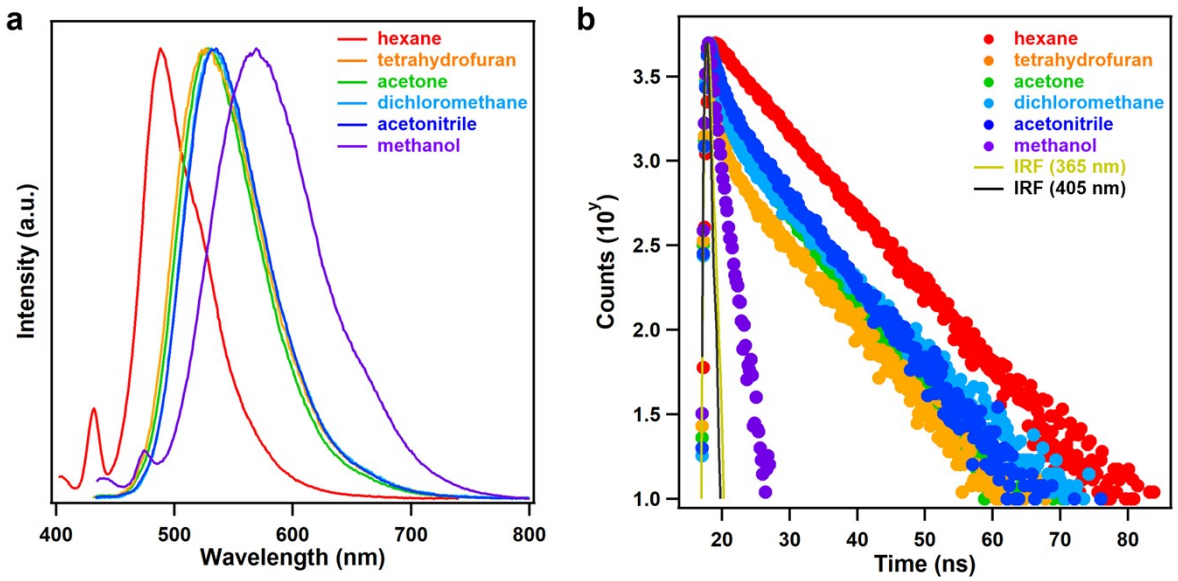

Figure S22. (a) Photoluminescence spectra and (b) photoluminescence decay profiles of PTz-TPB-COF dispersed in different organic solvents (excitation: 365 nm for hexane and 405 nm for other solvents).

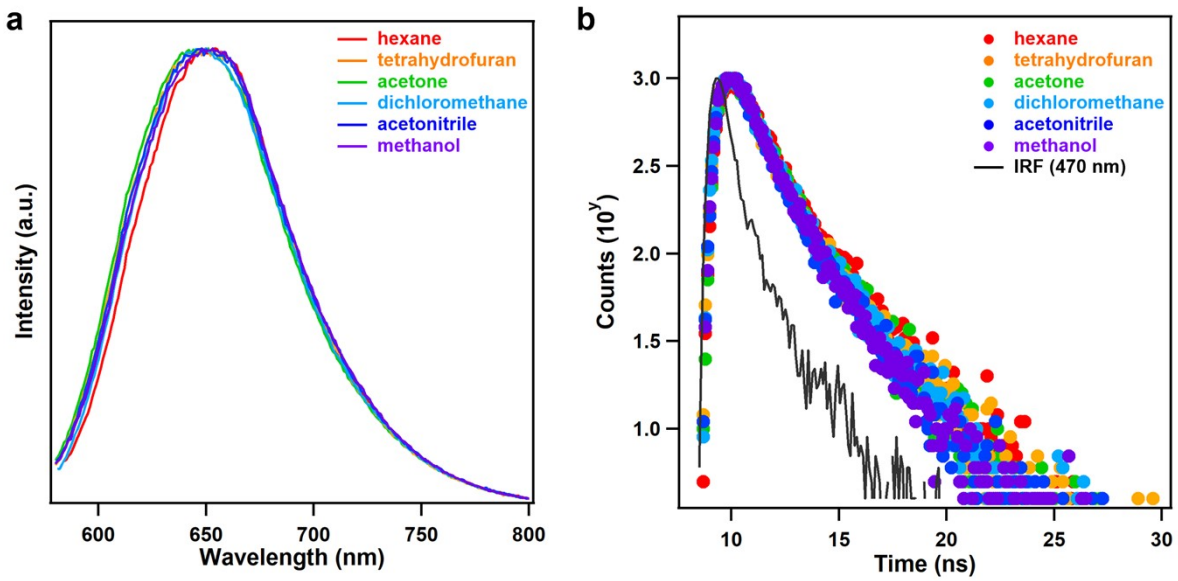

Figure S23. (a) Photoluminescence spectra and (b) photoluminescence decay profiles of PTz-BTA-COF dispersed in different organic solvents (excitation: 470 nm for each solvent).

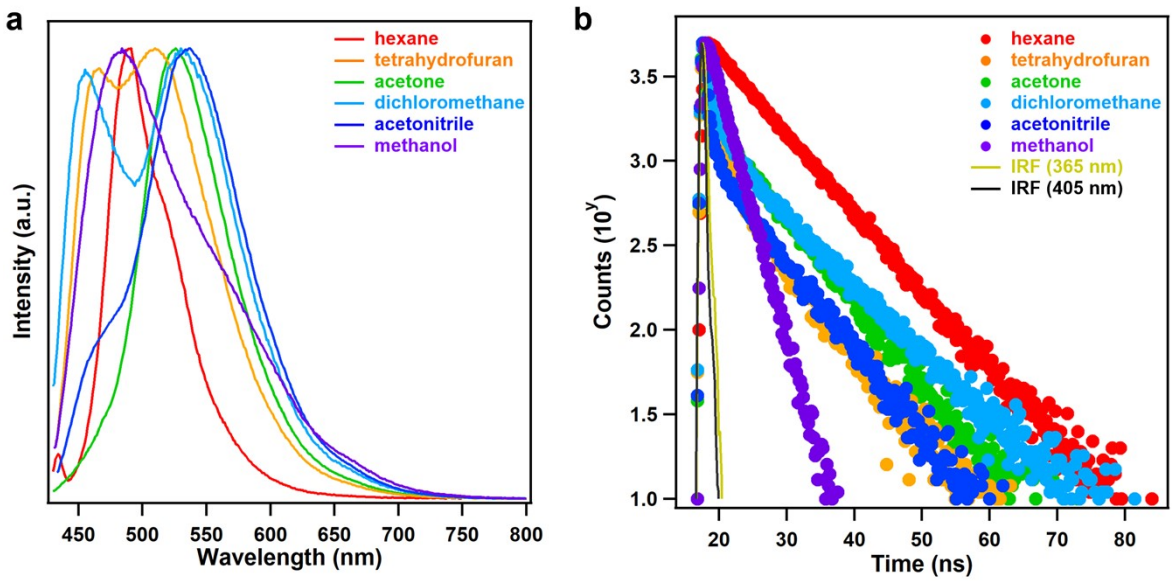

Figure S24. (a) Photoluminescence spectra and (b) photoluminescence decay profiles of PTz-Py-COF dispersed in different organic solvents (excitation: 365 nm for hexane and 405 nm for other solvents).

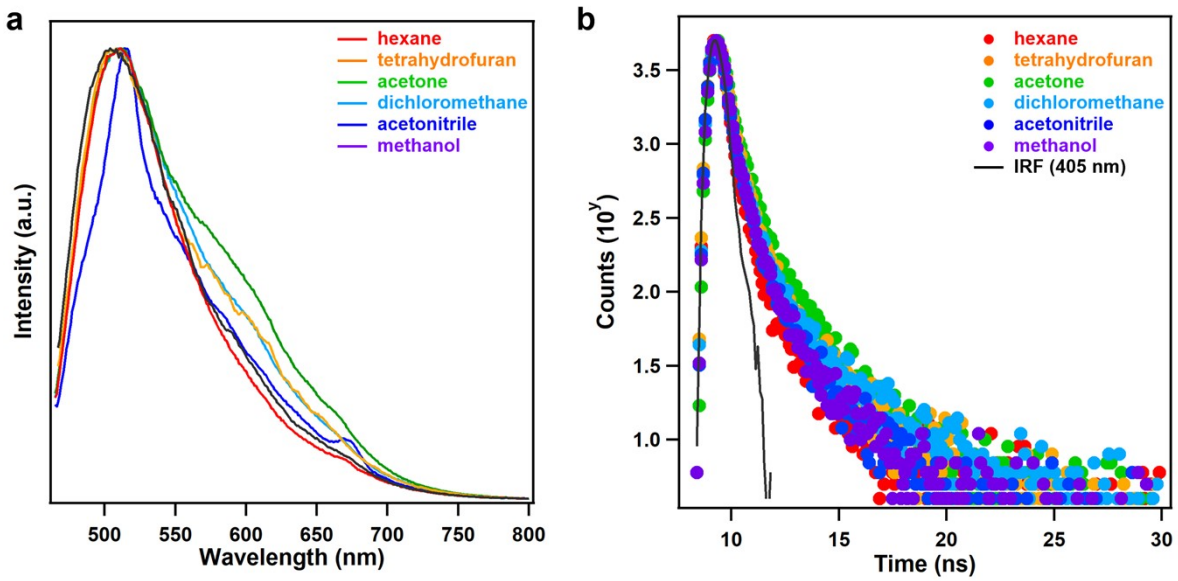

Figure S25. (a) Photoluminescence spectra and (b) photoluminescence decay profiles of OPTz-BTA-COF dispersed in different organic solvents (excitation: 405 nm for each solvent).

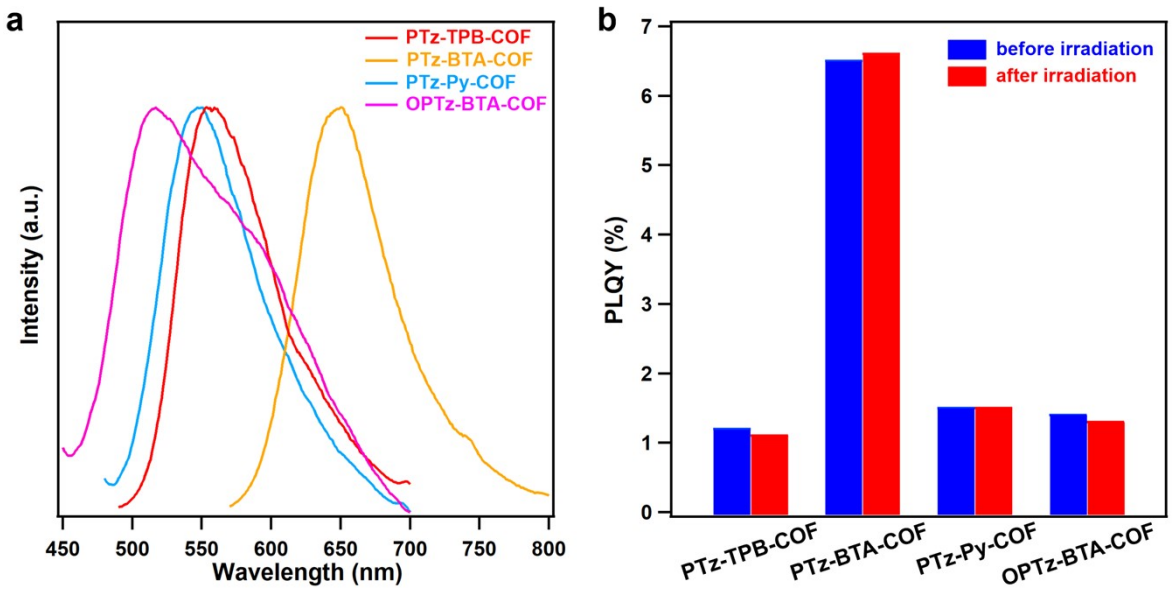

Figure S26. Photostability of the COFs. (a) Photoluminescence spectra after irradiation with a white-light Xe lamp (300 W) for 3 h in air. (b) PLQYs of the COFs before and after irradiation with a white-light Xe lamp (300 W) for 3 h in air.

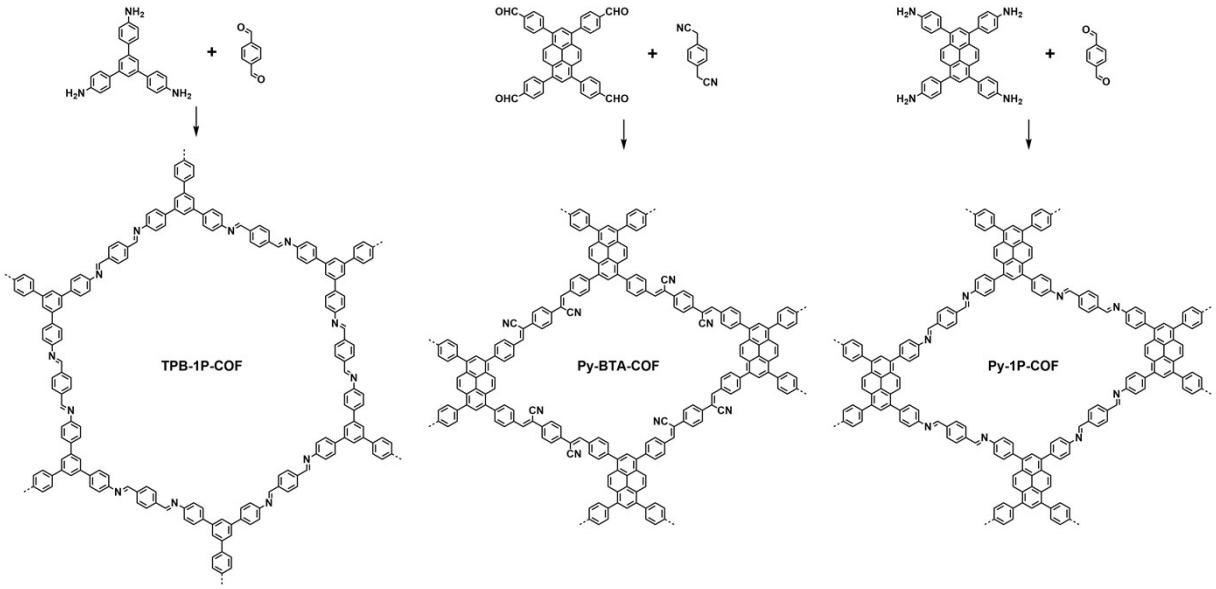

Figure S27. Synthesis of TPB-1P-COF, Py-BTA-COF, and Py-1P-COF.

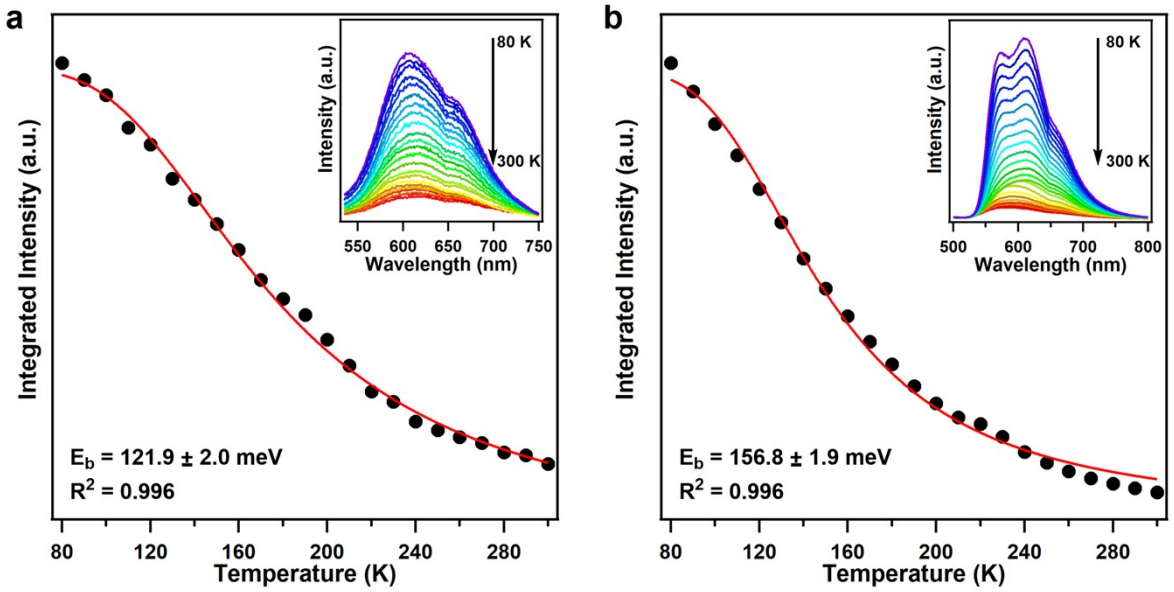

Figure S28. Integrated photoluminescence intensity as a function of temperature from 80 to 300 K of (a) Py-BTA-COF and (b) Py-1P-COF. The red curve represents the fitting by using the Arrhenius equation. The inset is the temperature-dependent photoluminescence spectra for each COF.

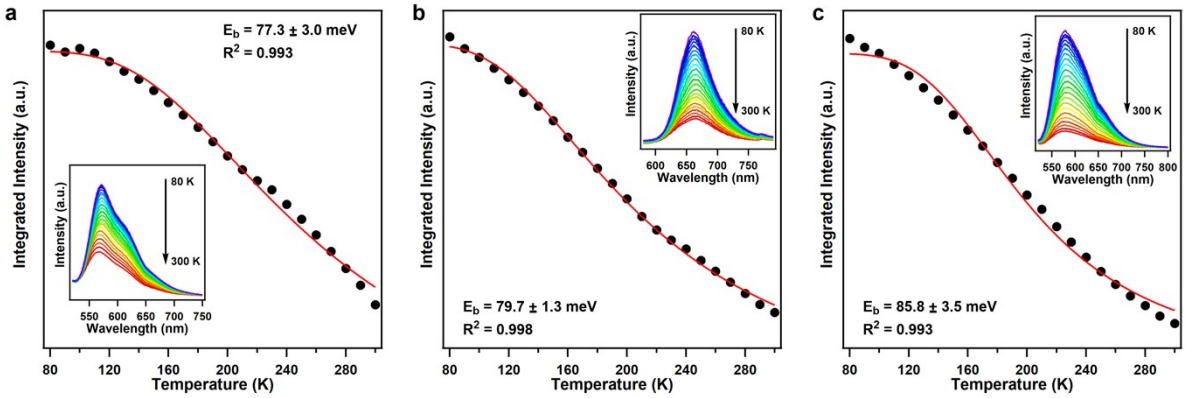

Figure S29. Integrated photoluminescence intensity as a function of temperature from 80 to 300 K of (a) PTz-TPB-CMP, (b) PTz-BTA-CMP, and (c) PTz-Py-CMP. The red curve represents the fitting by using the Arrhenius equation. The inset is the temperature-dependent photoluminescence spectra for each polymer.

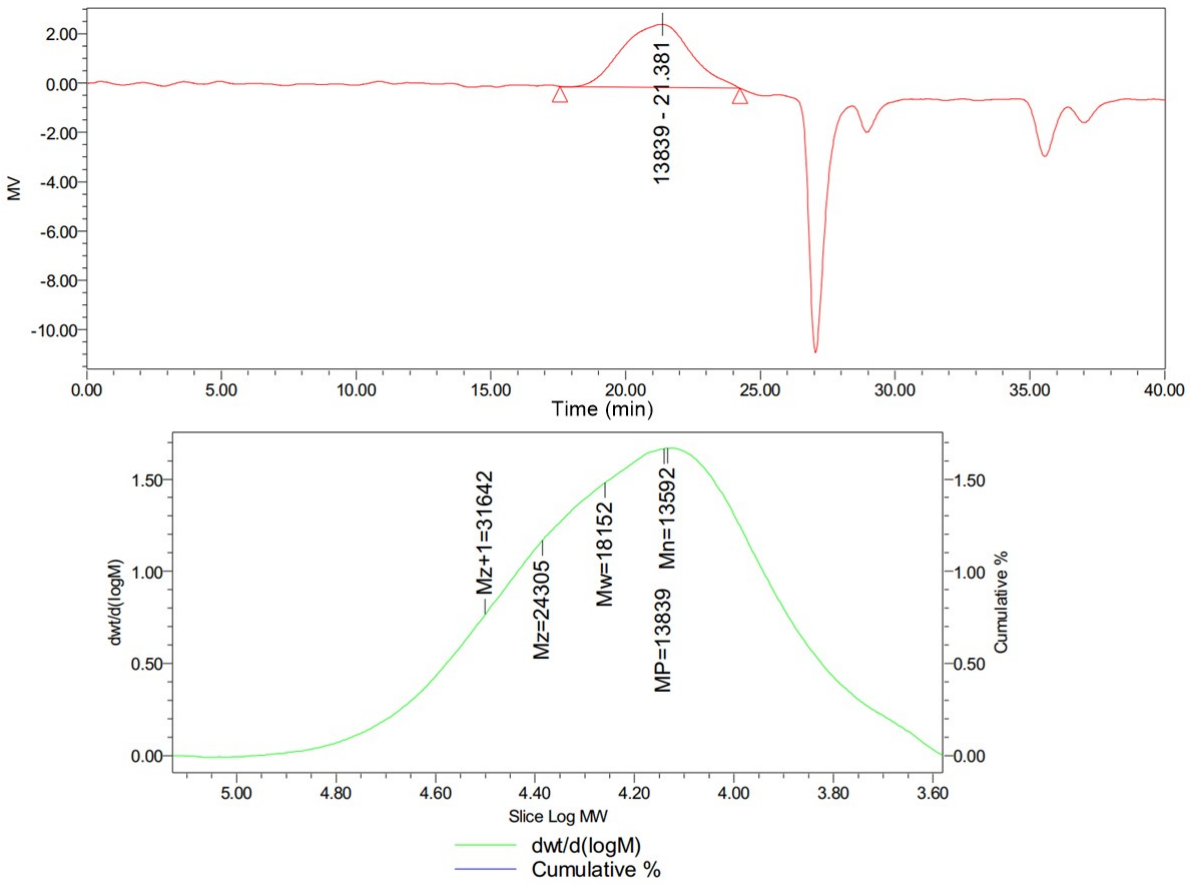

GPC result

	Mn	Mw	MP	Mz	Mz+1	Mv	*n*
1	13592	18152	13839	24305	31642		1.335528

Figure S30. GPC profile for the PMMA product after the polymerization reaction in a condition of Entry 1 in Table 1.

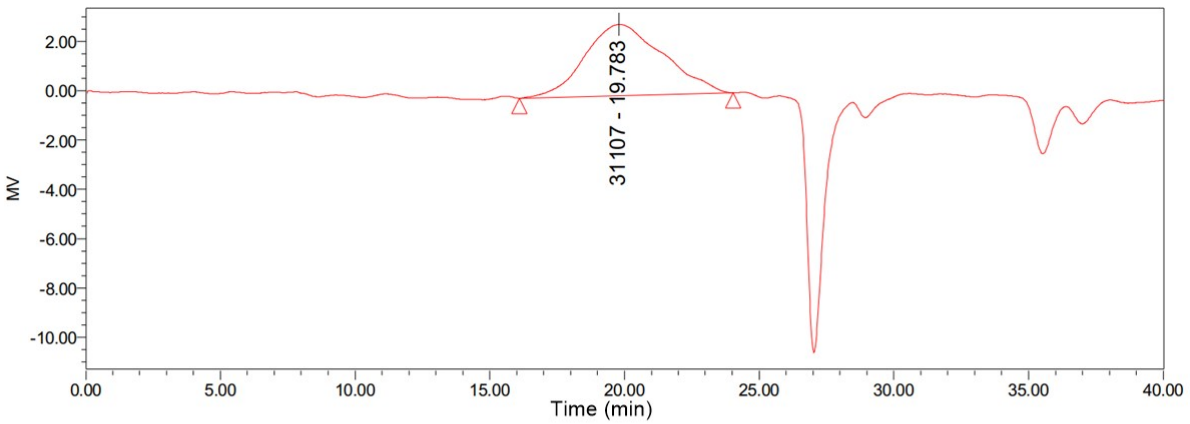

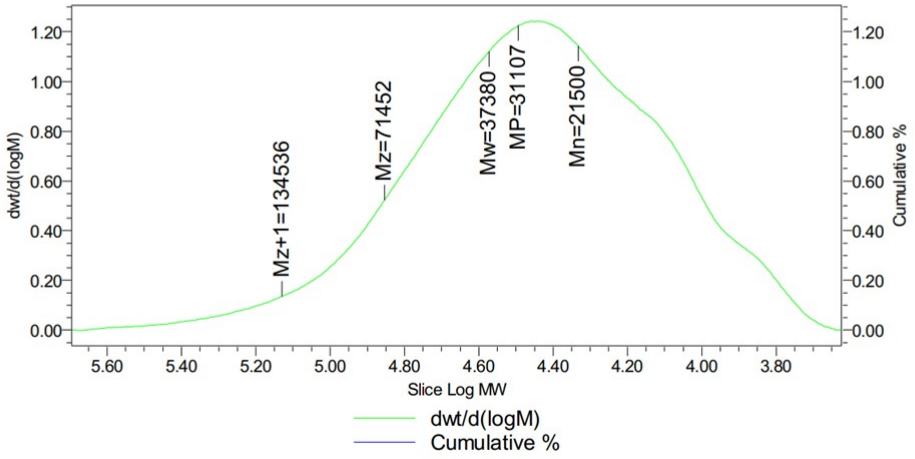

GPC result

	Mn	Mw	MP	Mz	Mz+1	Mv	*n*
1	21500	37380	31107	71452	134536		1.738562

Figure S31. GPC profile for the PMMA product after the polymerization reaction in a condition of Entry 2 in Table 1.

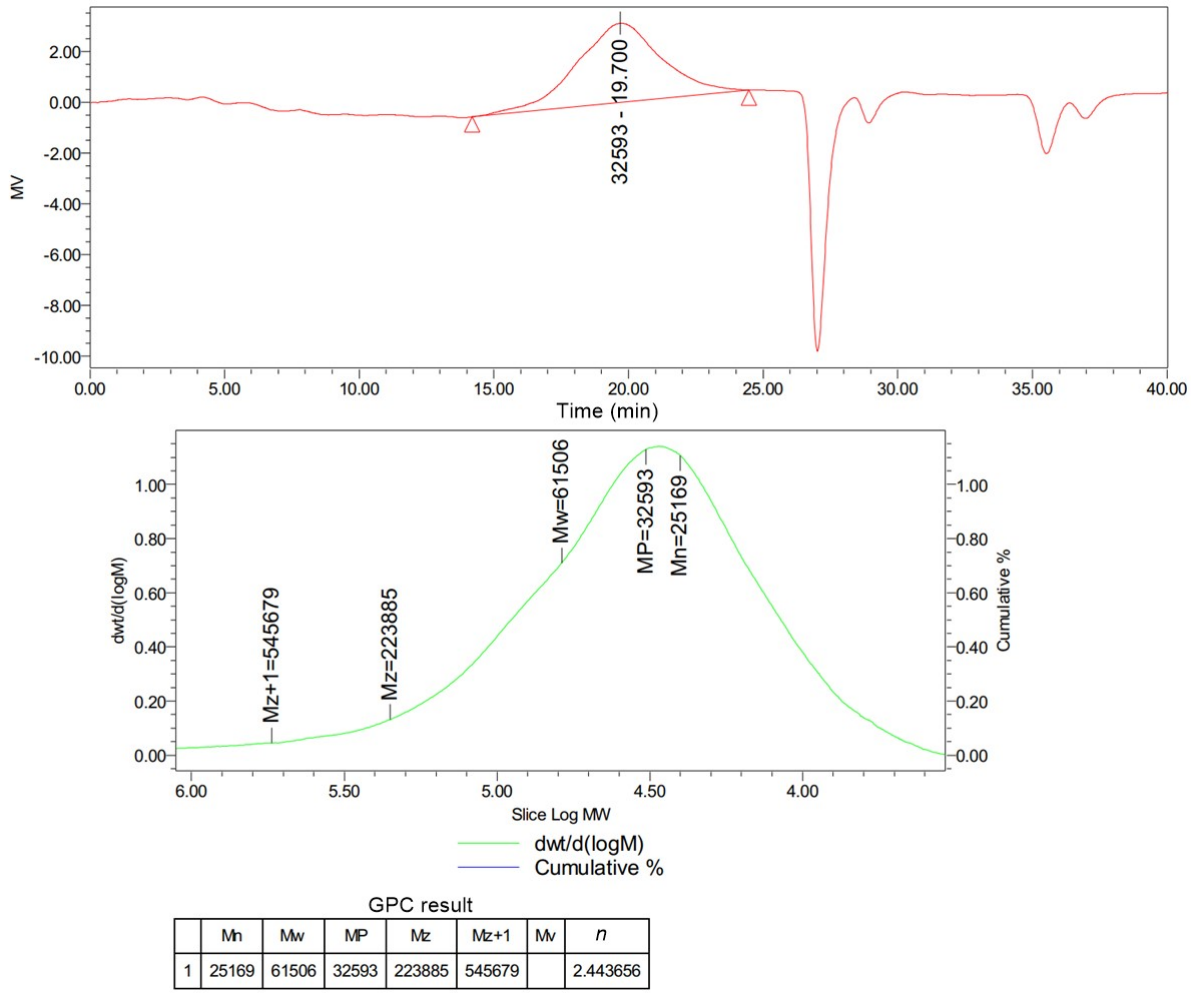

GPC result

	Mn	Mw	MP	Mz	Mz+1	Mv	*n*
1	25169	61506	32593	223885	545679		2.443656

Figure S32. GPC profile for the PMMA product after the polymerization reaction in a condition of Entry 3 in Table 1.

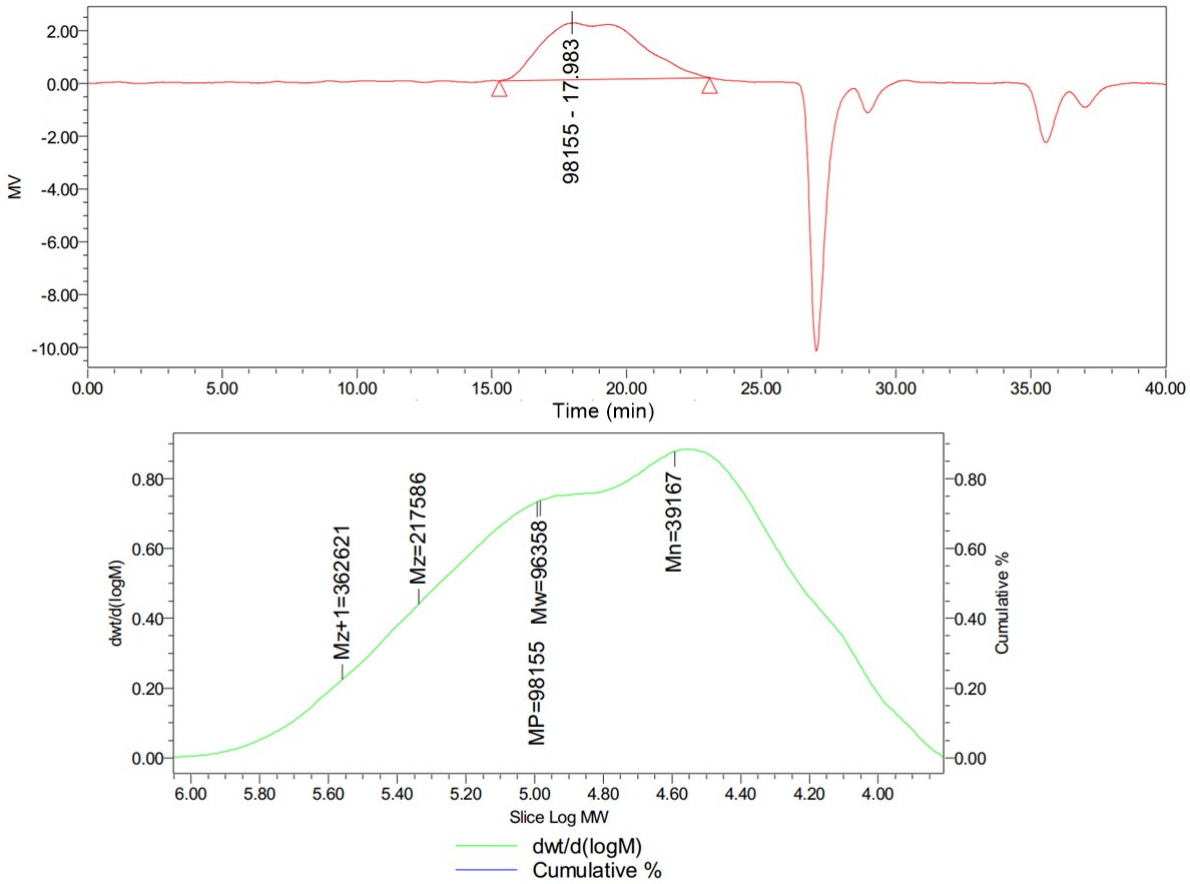

GPC result

	Mn	Mw	MP	Mz	Mz+1	Mv	*n*
1	39167	96358	98155	217586	362621		2.460164

Figure S33. GPC profile for the PMMA product after the polymerization reaction in a condition of Entry 4 in Table 1.

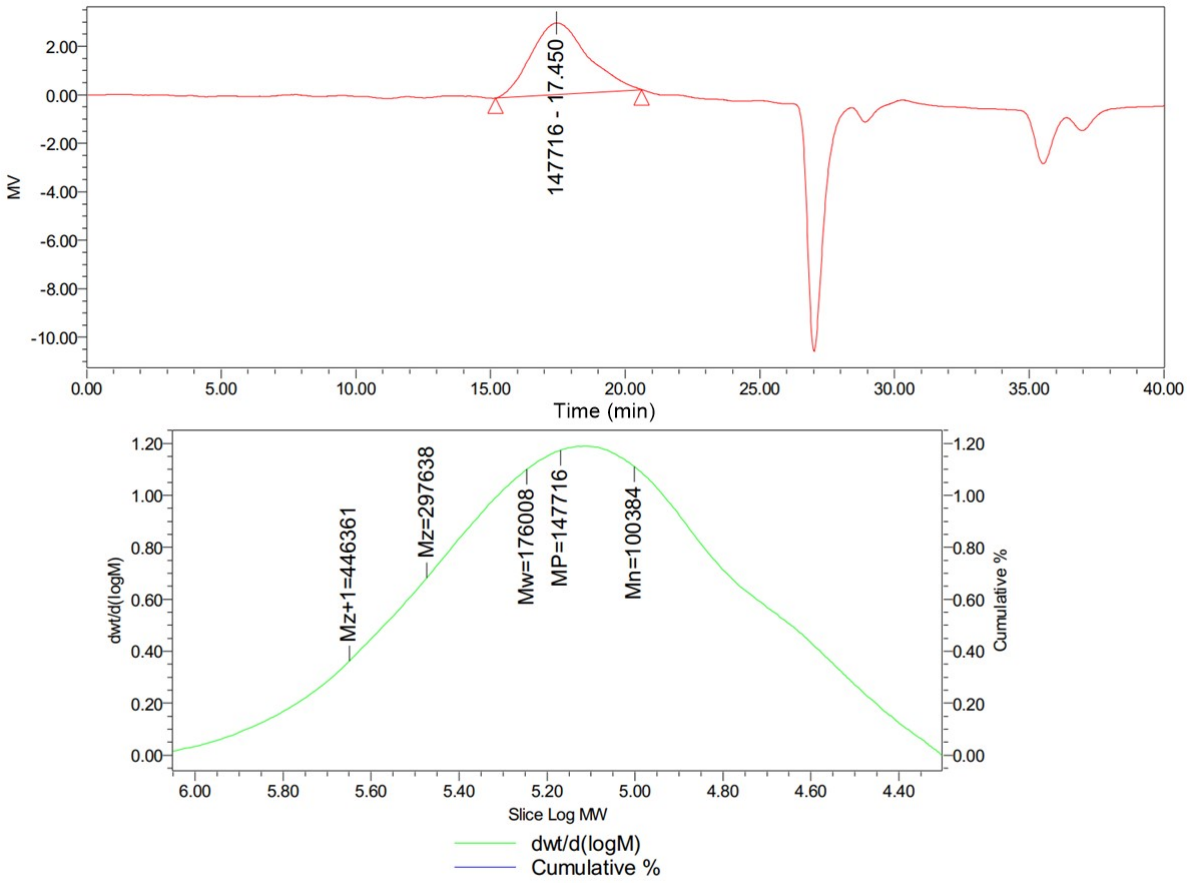

GPC result

	Mn	Mw	MP	Mz	Mz+1	Mv	*n*
1	100384	176008	147716	297638	446361		1.753347

Figure S34. GPC profile for the PMMA product after the polymerization reaction in a condition of Entry 5 in Table 1.

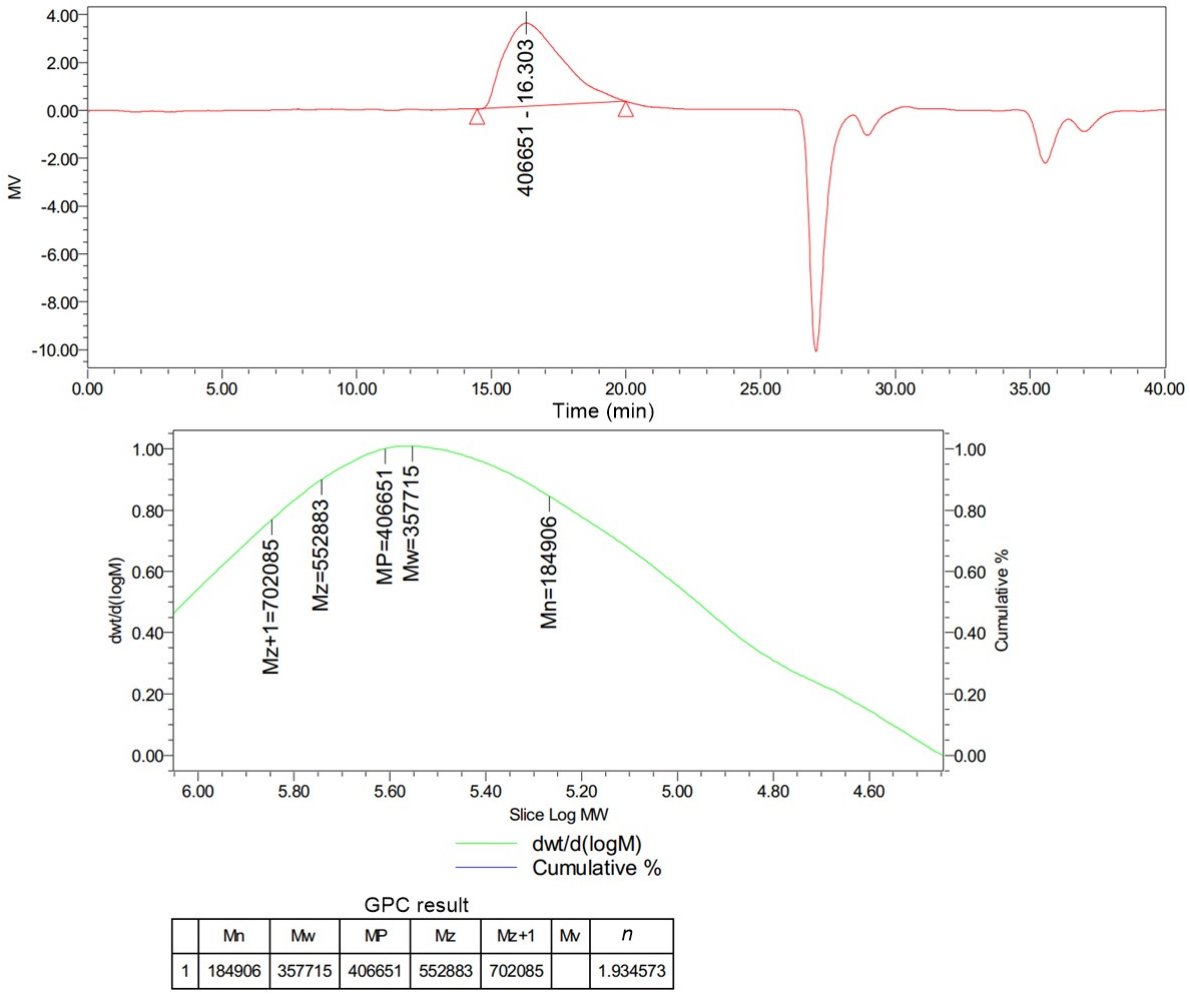

GPC result

	Mn	Mw	MP	Mz	Mz+1	Mv	*n*
1	184906	357715	406651	552883	702085		1.934573

Figure S35. GPC profile for the PMMA product after the polymerization reaction in a condition of Entry 6 in Table 1.

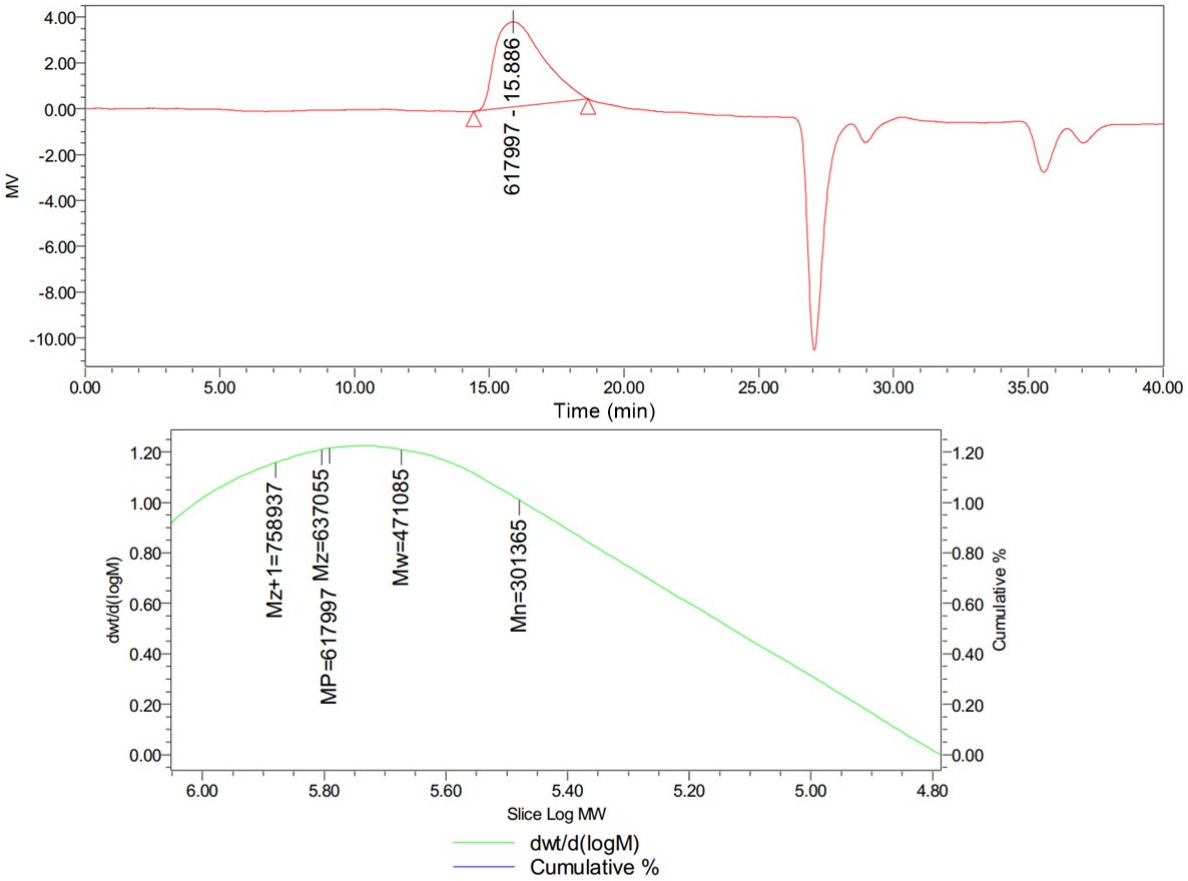

GPC result

	Mn	Mw	MP	Mz	Mz+1	Mv	*n*
1	301365	471085	617997	637055	758937		1.563170

Figure S36. GPC profile for the PMMA product after the polymerization reaction in a condition of Entry 7 in Table 1.

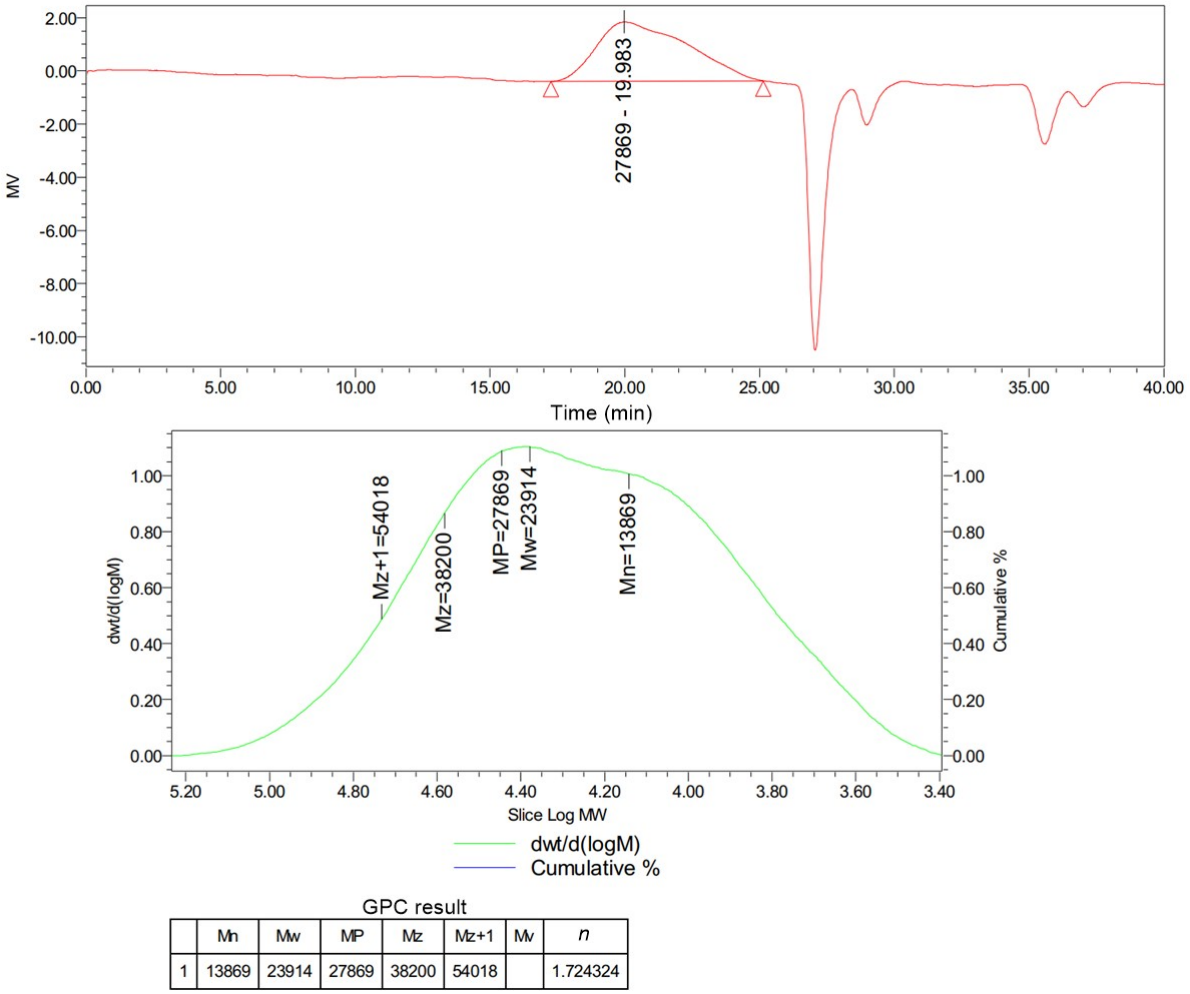

GPC result

	Mn	Mw	MP	Mz	Mz+1	Mv	n
1	13869	23914	27869	38200	54018		1.724324

Figure S37. GPC profile for the PMMA product after the polymerization reaction in a condition of Entry 8 in Table 1.

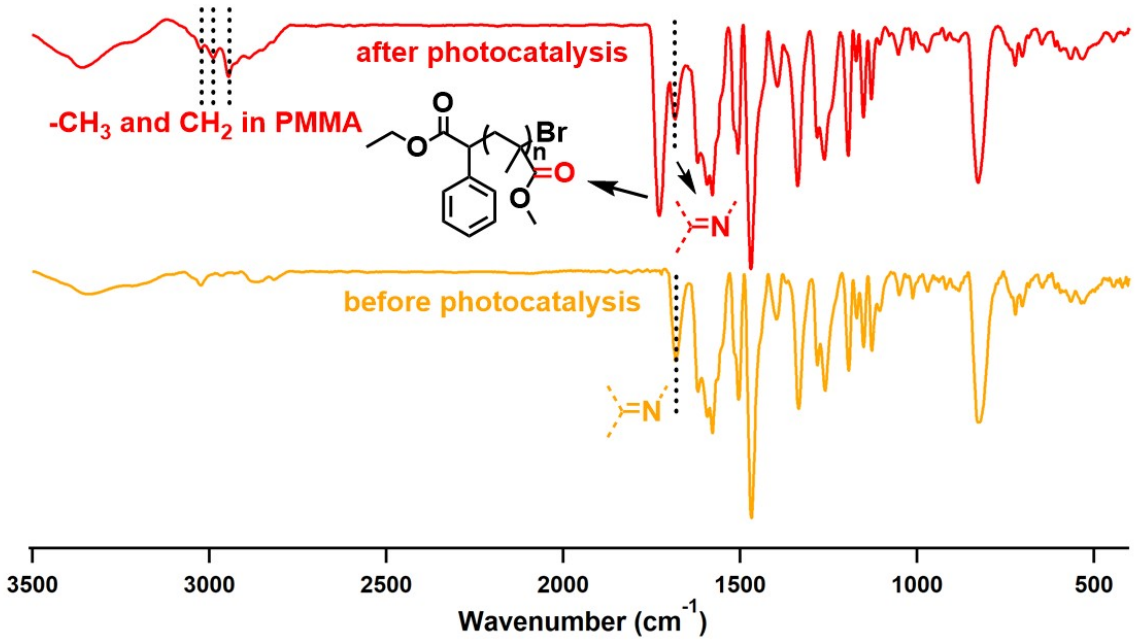

Figure S38. FT-IR spectra of PTz-TPB-COF before and after the polymerization reaction.

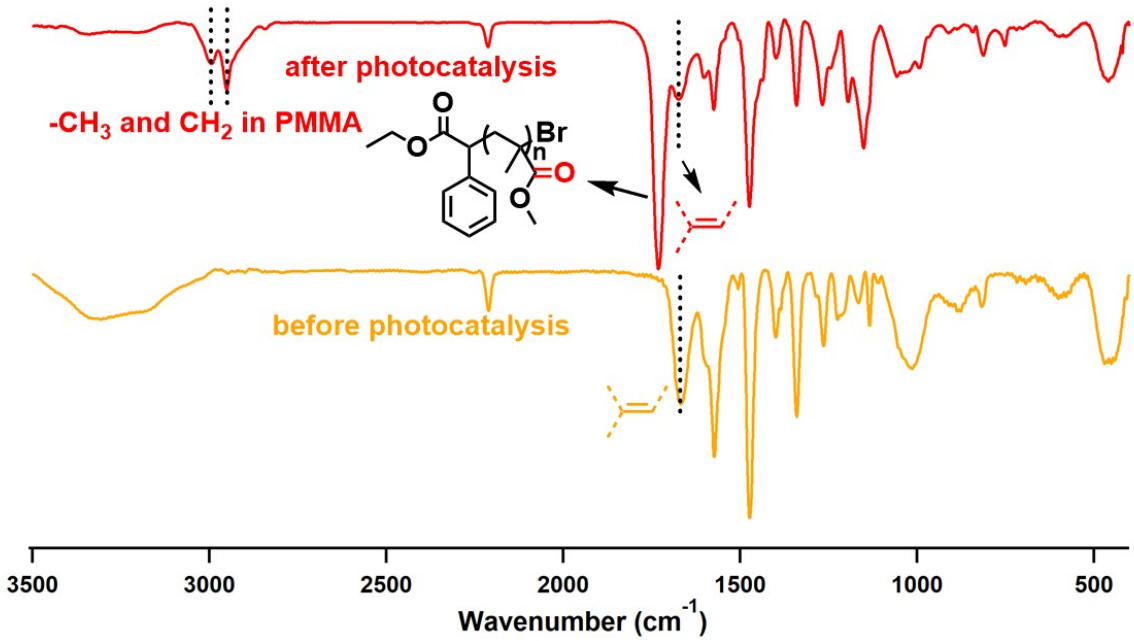

Figure S39. FT-IR spectra of PTz-BTA-COF before and after the polymerization reaction.

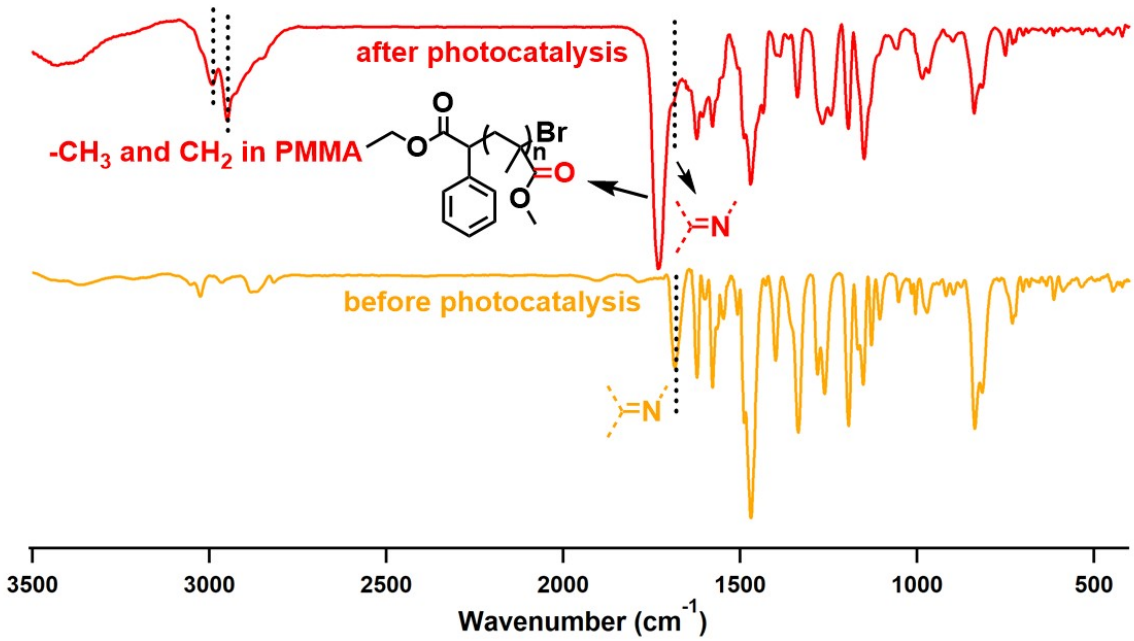

Figure S40. FT-IR spectra of PTz-Py-COF before and after the polymerization reaction.

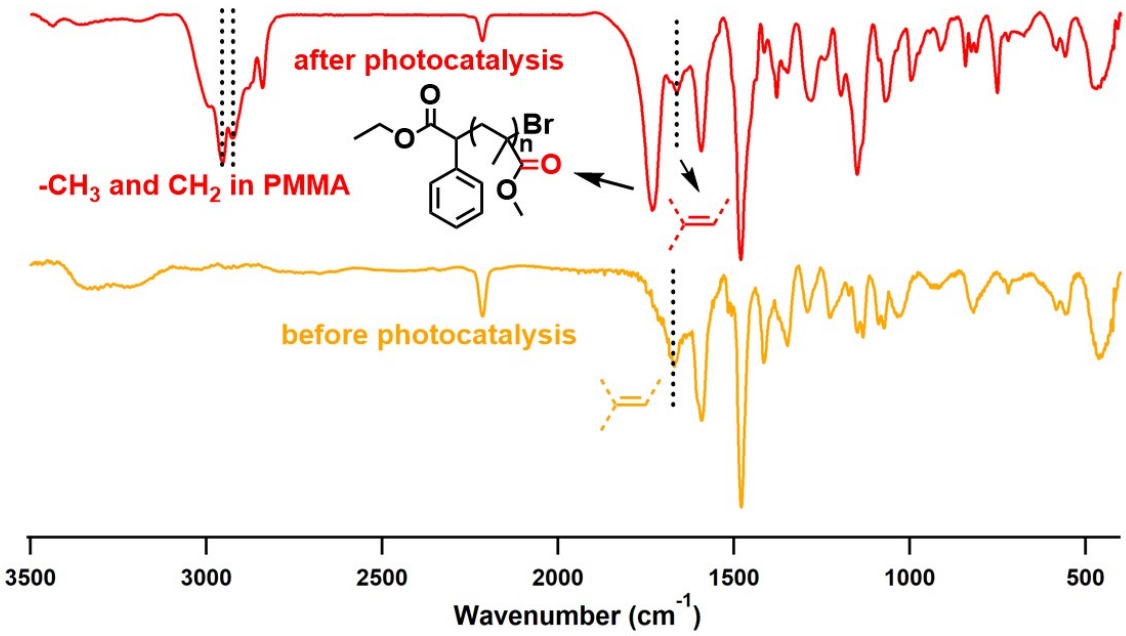

Figure S41. FT-IR spectra of OPTz-BTA-COF before and after the polymerization reaction.

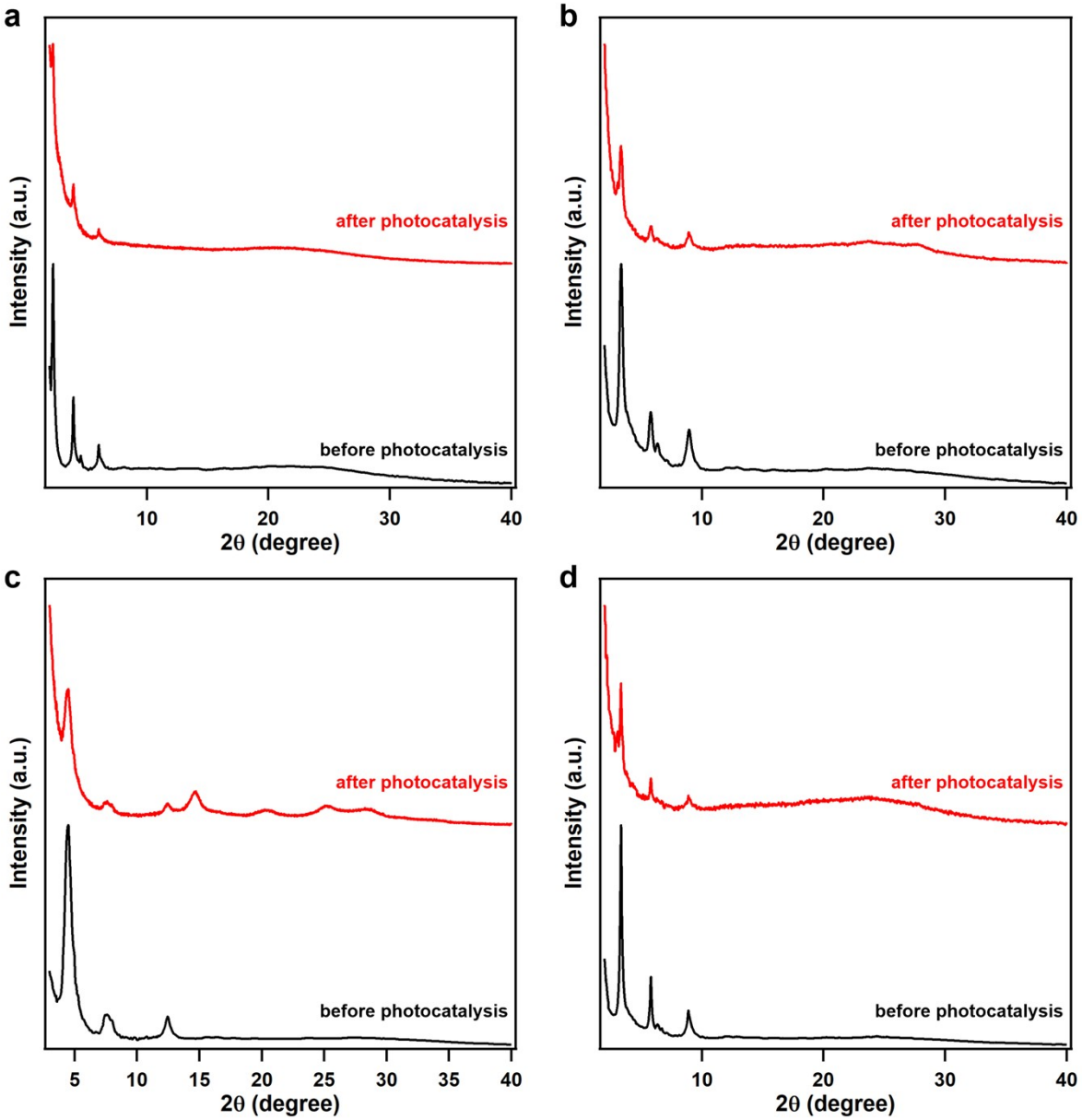

Figure S42. PXRD patterns of (a) PTz-TPB-COF, (b) PTz-BTA-COF, (c) PTz-Py-COF, and (d) OPTz-BTA-COF before and after the photocatalytic polymerization reactions.

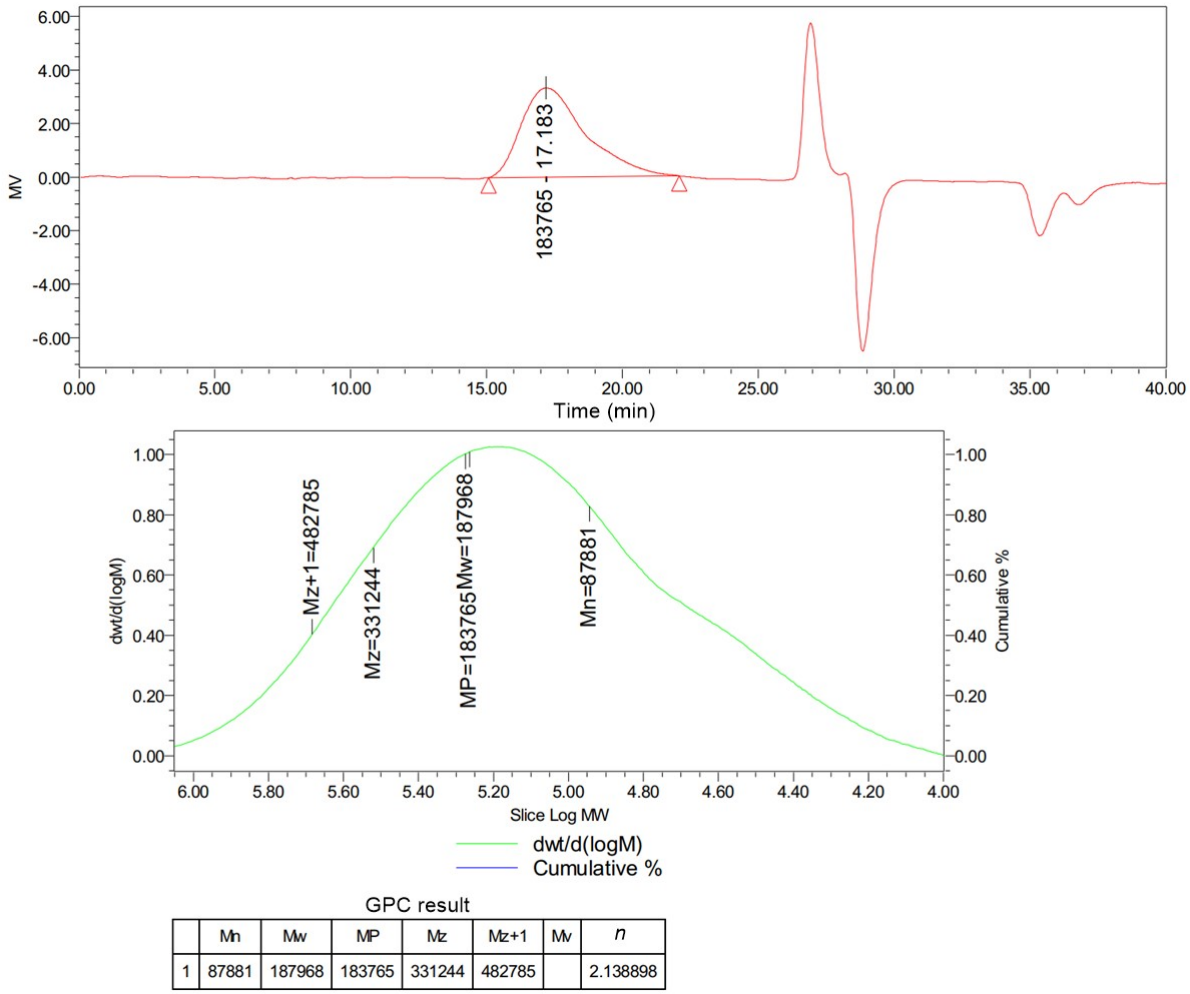

GPC result

	Mn	Mw	MP	Mz	Mz+1	Mv	*n*
1	87881	187968	183765	331244	482785		2.138898

Figure S43. GPC profile for the PMMA product after the polymerization reaction in a condition of Entry 9 in Table 1.

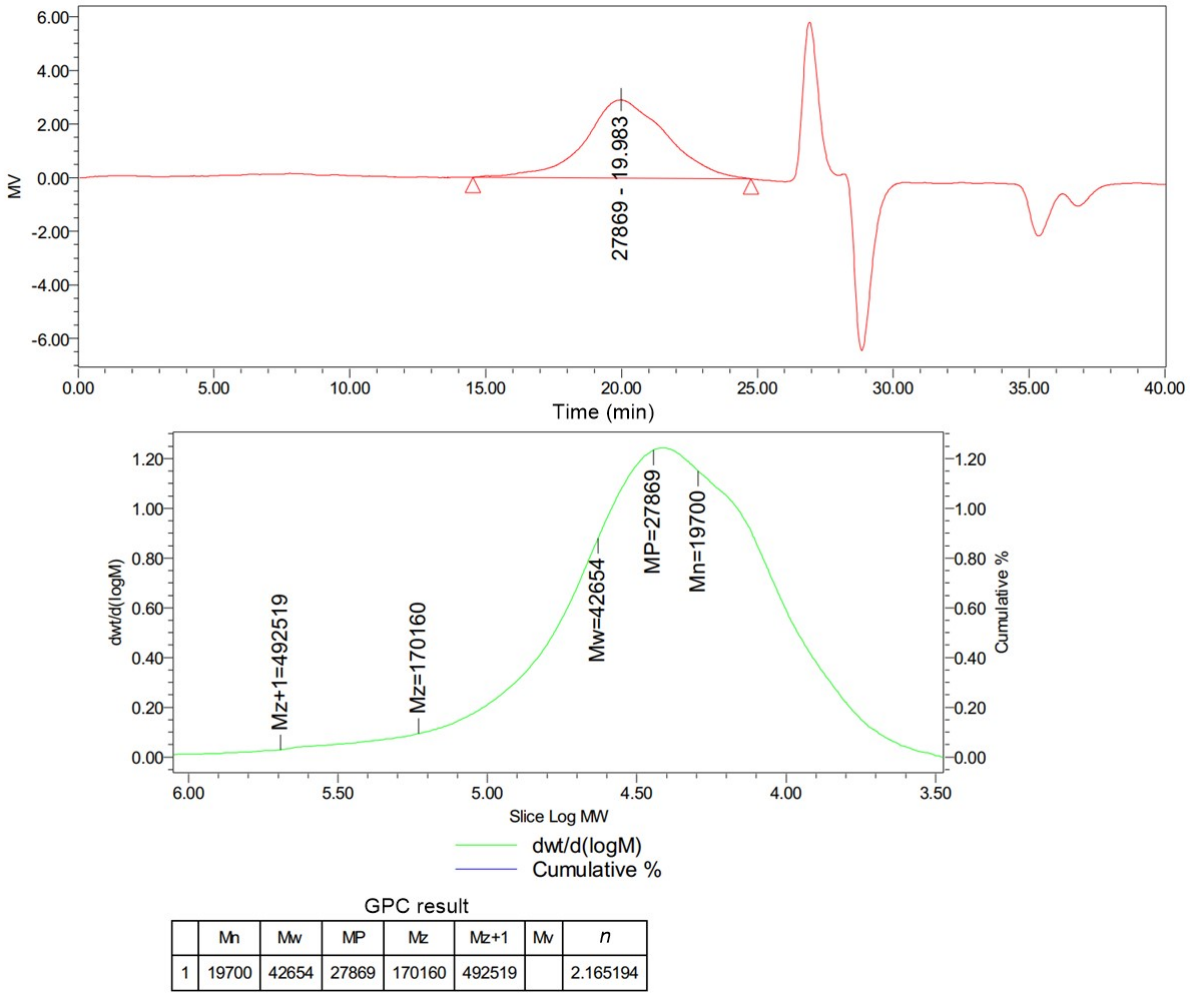

GPC result

	Mn	Mw	MP	Mz	Mz+1	Mv	n
1	19700	42654	27869	170160	492519		2.165194

Figure S44. GPC profile for the PMMA product after the polymerization reaction in a condition of Entry 10 in Table 1.

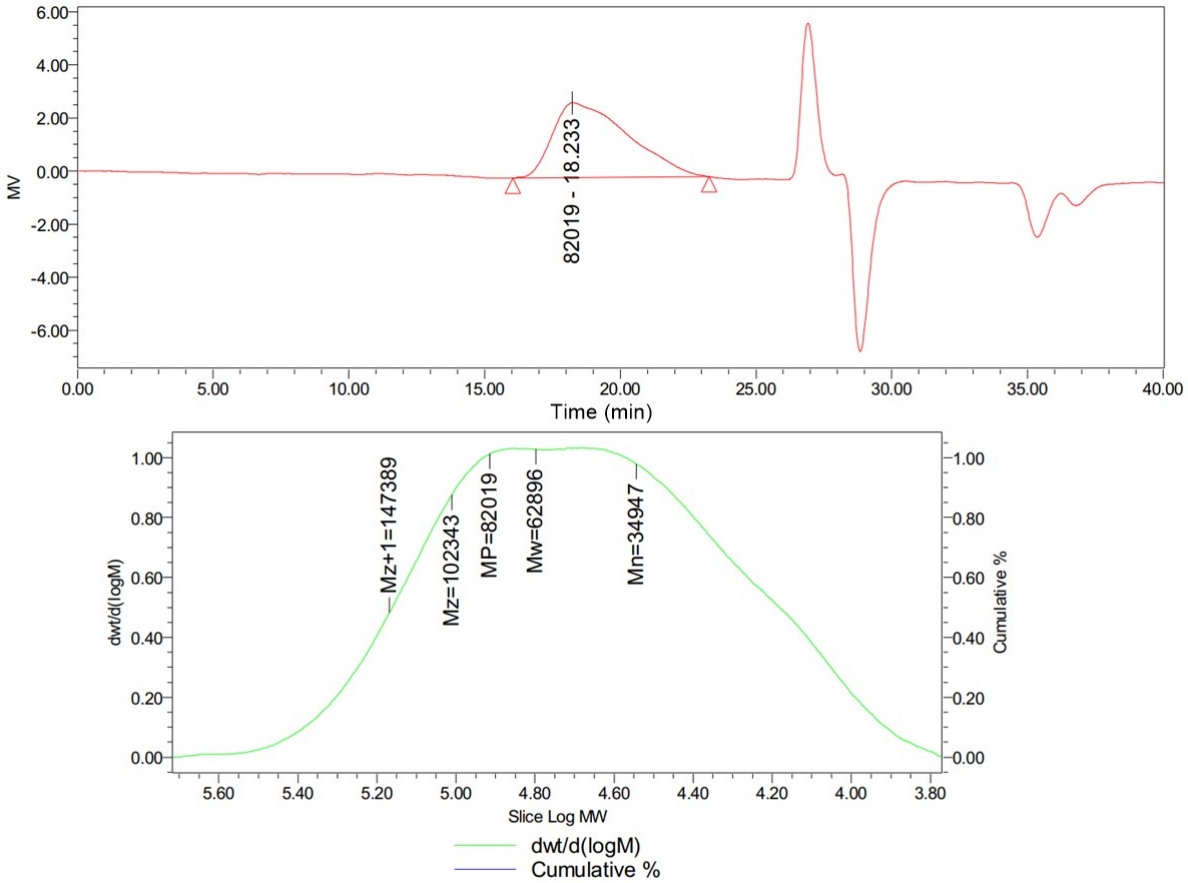

GPC result

	Mn	Mw	MP	Mz	Mz+1	Mv	*n*
1	34947	62896	82019	102343	147389		1.799763

Figure S45. GPC profile for the PMMA product after the polymerization reaction in a condition of Entry 11 in Table 1.

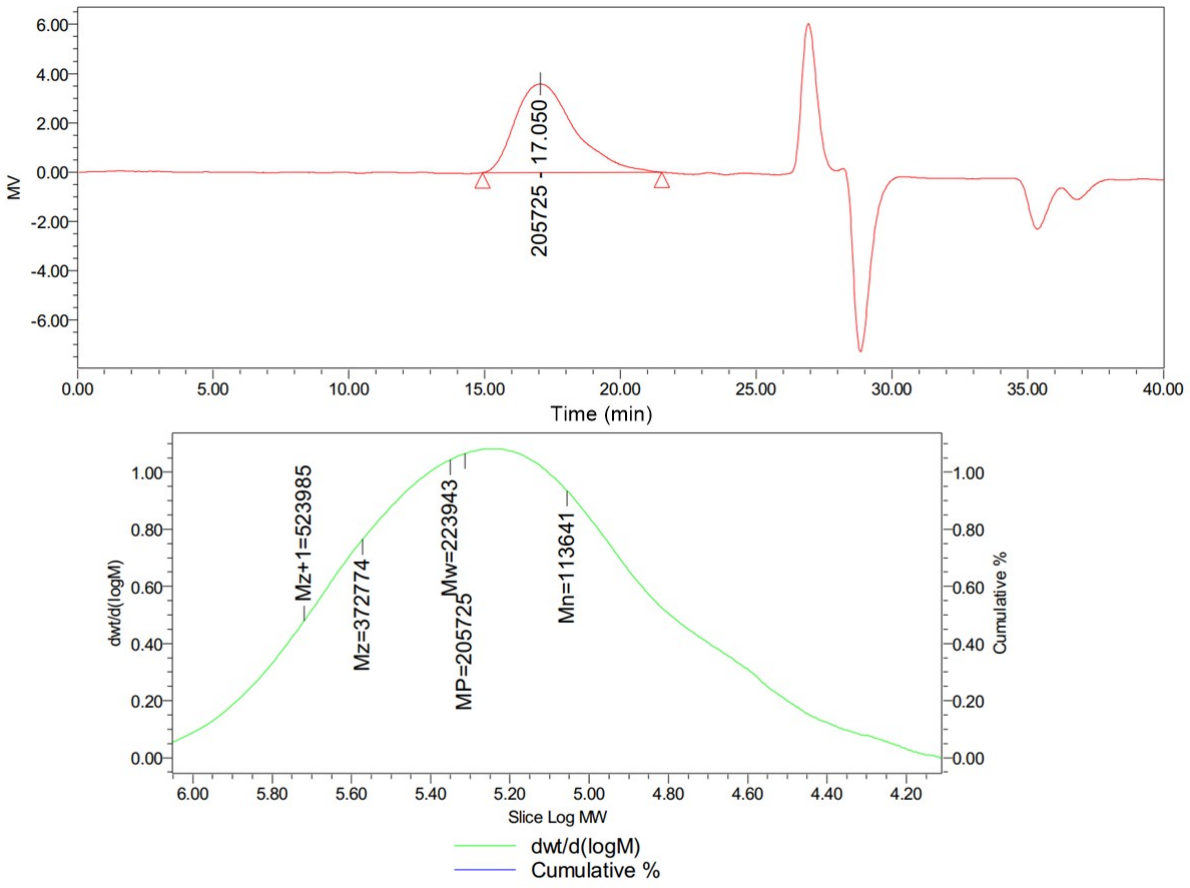

GPC result

	Mn	Mw	MP	Mz	Mz+1	Mv	*n*
1	113641	223943	205725	372774	523985		1.970609

Figure S46. GPC profile for the PMMA product after the polymerization reaction in a condition of Entry 12 in Table 1.

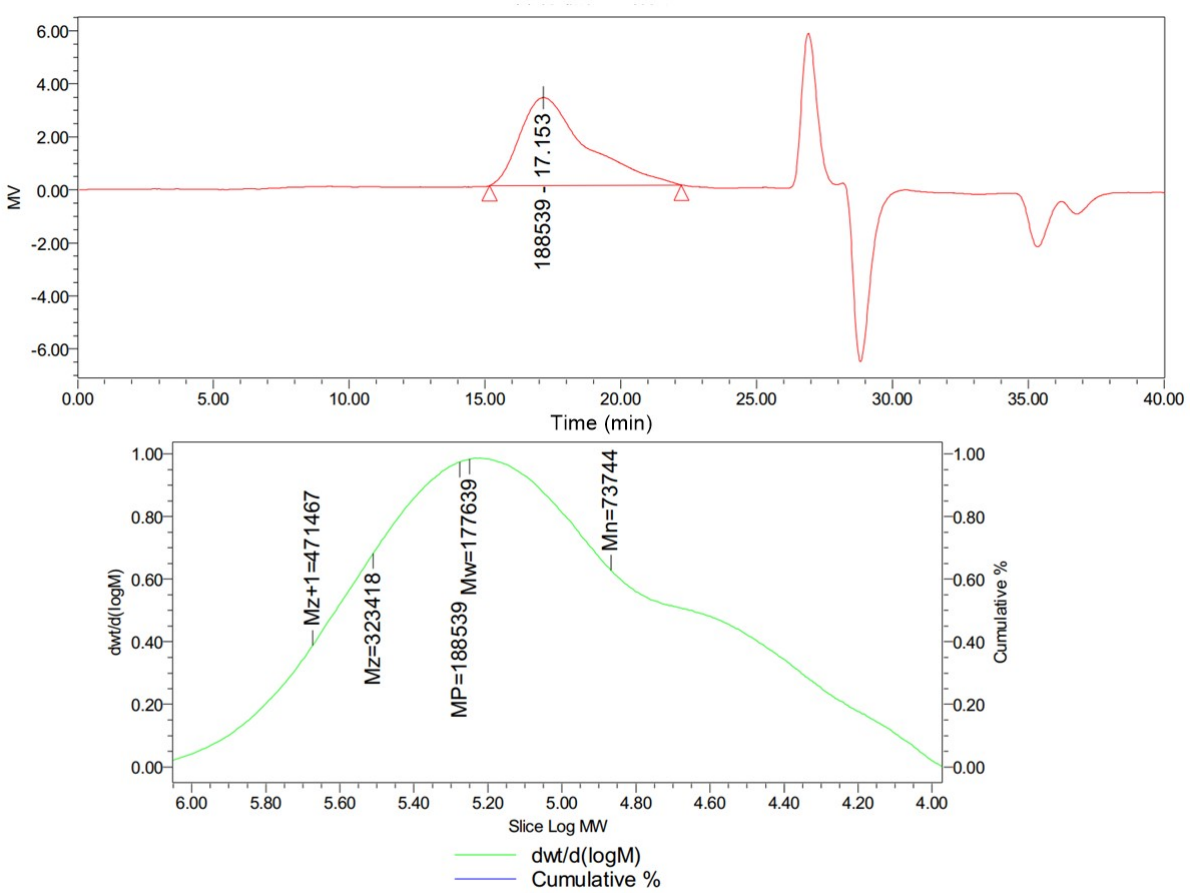

GPC result

	Mn	Mw	MP	Mz	Mz+1	Mv	*n*
1	73744	177639	188539	323418	471467		2.408871

Figure S47. GPC profile for the PMMA product after the polymerization reaction in a condition of Entry 13 in Table 1.

Supporting Tables

Table S1. Screening of conditions for COF synthesis.

Reactant 1 (15.35 mg)	Reactant 2 (13.36 mg)	Acid (0.1 mL)	Solvent (1 mL)	Ratio	Temperature (ºC)	Time (d)	Result
MPTz	TAPB	6 M AcOH	*o*-DCB/*n*-BuOH	1/9	120	3	Amorphous
MPTz	TAPB	6 M AcOH	*o*-DCB/*n*-BuOH	1/4	120	3	Amorphous
MPTz	TAPB	6 M AcOH	*o*-DCB/*n*-BuOH	3/7	120	3	Amorphous
MPTz	TAPB	6 M AcOH	*o*-DCB/*n*-BuOH	2/3	120	3	Poorly crystalline
MPTz	TAPB	6 M AcOH	*o*-DCB/*n*-BuOH	1/1	120	3	Poorly crystalline
MPTz	TAPB	6 M AcOH	*o*-DCB/*n*-BuOH	3/2	120	3	Poorly crystalline
MPTz	TAPB	6 M AcOH	*o*-DCB/*n*-BuOH	7/3	120	3	Poorly crystalline
MPTz	TAPB	6 M AcOH	*o*-DCB/*n*-BuOH	4/1	120	3	Amorphous
MPTz	TAPB	6 M AcOH	*o*-DCB/*n*-BuOH	9/1	120	3	Amorphous
MPTz	TAPB	6 M AcOH	*o*-DCB	-	120	3	Amorphous
MPTz	TAPB	6 M AcOH	*o*-DCB/*n*-BuOH	1/9	120	7	Amorphous
MPTz	TAPB	6 M AcOH	*o*-DCB/*n*-BuOH	1/4	120	7	Amorphous
MPTz	TAPB	6 M AcOH	*o*-DCB/*n*-BuOH	3/7	120	7	Amorphous
MPTz	TAPB	6 M AcOH	*o*-DCB/*n*-BuOH	2/3	120	7	Amorphous
MPTz	TAPB	6 M AcOH	*o*-DCB/*n*-BuOH	1/1	120	7	Poorly crystalline
MPTz	TAPB	6 M AcOH	*o*-DCB/*n*-BuOH	3/2	120	7	Poorly crystalline
MPTz	TAPB	6 M AcOH	*o*-DCB/*n*-BuOH	7/3	120	7	Amorphous
MPTz	TAPB	6 M AcOH	*o*-DCB/*n*-BuOH	4/1	120	7	Amorphous
MPTz	TAPB	6 M AcOH	*o*-DCB/*n*-BuOH	9/1	120	7	Amorphous
MPTz	TAPB	6 M AcOH	*o*-DCB	-	120	7	Amorphous
MPTz	TAPB	6 M AcOH	mesitylene	-	120	3	Crystalline
MPTz	TAPB	6 M AcOH	dioxane/mesitylene	1/9	120	3	Crystalline
MPTz	TAPB	6 M AcOH	dioxane/mesitylene	1/4	120	3	Highly crystalline
MPTz	TAPB	6 M AcOH	dioxane/mesitylene	3/7	120	3	Crystalline
MPTz	TAPB	6 M AcOH	dioxane/mesitylene	2/3	120	3	Crystalline
MPTz	TAPB	6 M AcOH	dioxane/mesitylene	1/1	120	3	Crystalline
MPTz	TAPB	6 M AcOH	dioxane/mesitylene	3/2	120	3	Poorly crystalline
MPTz	TAPB	6 M AcOH	dioxane/mesitylene	7/3	120	3	Poorly crystalline
MPTz	TAPB	6 M AcOH	dioxane/mesitylene	4/1	120	3	Amorphous
MPTz	TAPB	6 M AcOH	dioxane/mesitylene	9/1	120	3	Amorphous
MPTz	TAPB	6 M AcOH	dioxane	-	120	3	Amorphous
MPTz	TAPB	6 M AcOH	mesitylene	-	120	7	Crystalline
MPTz	TAPB	6 M AcOH	dioxane/mesitylene	1/9	120	7	Crystalline
MPTz	TAPB	6 M AcOH	dioxane/mesitylene	1/4	120	7	Crystalline
MPTz	TAPB	6 M AcOH	dioxane/mesitylene	3/7	120	7	Crystalline
MPTz	TAPB	6 M AcOH	dioxane/mesitylene	2/3	120	7	Poorly crystalline
MPTz	TAPB	6 M AcOH	dioxane/mesitylene	1/1	120	7	Poorly crystalline
MPTz	TAPB	6 M AcOH	dioxane/mesitylene	3/2	120	7	Amorphous
MPTz	TAPB	6 M AcOH	dioxane/mesitylene	7/3	120	7	Amorphous
MPTz	TAPB	6 M AcOH	dioxane/mesitylene	4/1	120	7	Amorphous
MPTz	TAPB	6 M AcOH	dioxane/mesitylene	9/1	120	7	Amorphous
MPTz	TAPB	6 M AcOH	dioxane	-	120	7	Amorphous
Reactant 1 (15.35 mg)	Reactant 2 (7.42 mg)	Base	Solvent (1 mL)	Ratio	Temperature (ºC)	Time (d)	Result
MPTz	BTTA	0.1 mL 4 M KOH	*o*-DCB	-	120	3	No product
MPTz	BTTA	0.1 mL 4 M KOH	*o*-DCB/*n*-BuOH	1/1	120	3	Amorphous
MPTz	BTTA	0.1 mL 4 M KOH	*o*-DCB/DMA	1/1	120	3	Amorphous
MPTz	BTTA	0.1 mL 4 M KOH	*n*-BuOH	-	120	3	Highly crystalline
MPTz	BTTA	0.1 mL 4 M KOH	DMA	-	120	3	Amorphous
MPTz	BTTA	0.1 mL 4 M KOH	dioxane	-	120	3	Amorphous
MPTz	BTTA	0.1 mL 4 M KOH	dioxane/mesitylene	1/1	120	3	Amorphous
MPTz	BTTA	0.1 mL 4 M KOH	dioxane/DMA	1/1	120	3	Amorphous

MPTz	BTTA	0.1 mL 4 M KOH	mesitylene/DMA	1/1	120	3	Amorphous
MPTz	BTTA	0.1 mL 4 M KOH	*n*-BuOH/*o*-DCB	9/1	120	3	Crystalline
MPTz	BTTA	0.1 mL 4 M KOH	*n*-BuOH/DMA	9/1	120	3	Amorphous
MPTz	BTTA	0.1 mL 4 M KOH	*n*-BuOH/dioxane	9/1	120	3	Amorphous
MPTz	BTTA	0.1 mL 4 M KOH	*n*-BuOH/mesitylene	9/1	120	3	Crystalline
MPTz	BTTA	0.1 mL 4 M KOH	*n*-BuOH/ACN	9/1	120	3	Amorphous
MPTz	BTTA	0.1 mL 4 M KOH	*n*-BuOH/NMP	9/1	120	3	Amorphous
MPTz	BTTA	36 mg Cs_2CO_3	dioxane	-	120	3	Amorphous
MPTz	BTTA	36 mg Cs_2CO_3	dioxane/mesitylene	1/1	120	3	Amorphous
MPTz	BTTA	36 mg Cs_2CO_3	mesitylene	-	120	3	Amorphous
MPTz	BTTA	36 mg Cs_2CO_3	*o*-DCB	-	120	3	Amorphous
MPTz	BTTA	36 mg Cs_2CO_3	*o*-DCB/*n*-BuOH	1/1	120	3	Amorphous
MPTz	BTTA	36 mg Cs_2CO_3	*n*-BuOH	-	120	3	Amorphous

Reactant 1 (15.08 mg)	Reactant 2 (15.87 mg)	Acid (0.1 mL)	Solvent (1 mL)	Ratio	Temperature (ºC)	Time (d)	Result
MPTz	TAPP	6 M AcOH	*o*-DCB/*n*-BuOH	1/9	120	3	Crystalline
MPTz	TAPP	6 M AcOH	*o*-DCB/*n*-BuOH	1/4	120	3	Crystalline
MPTz	TAPP	6 M AcOH	*o*-DCB/*n*-BuOH	3/7	120	3	Crystalline
MPTz	TAPP	6 M AcOH	*o*-DCB/*n*-BuOH	2/3	120	3	Crystalline
MPTz	TAPP	6 M AcOH	*o*-DCB/*n*-BuOH	1/1	120	3	Poorly crystalline
MPTz	TAPP	6 M AcOH	*o*-DCB/*n*-BuOH	3/2	120	3	Poorly crystalline
MPTz	TAPP	6 M AcOH	*o*-DCB/*n*-BuOH	7/3	120	3	Highly crystalline
MPTz	TAPP	6 M AcOH	*o*-DCB/*n*-BuOH	4/1	120	3	Poorly crystalline
MPTz	TAPP	6 M AcOH	*o*-DCB/*n*-BuOH	9/1	120	3	Poorly crystalline
MPTz	TAPP	6 M AcOH	*o*-DCB	-	120	3	Crystalline
MPTz	TAPP	6 M AcOH	*o*-DCB/*n*-BuOH	1/9	120	7	Amorphous
MPTz	TAPP	6 M AcOH	*o*-DCB/*n*-BuOH	1/4	120	7	Amorphous
MPTz	TAPP	6 M AcOH	*o*-DCB/*n*-BuOH	3/7	120	7	Amorphous
MPTz	TAPP	6 M AcOH	*o*-DCB/*n*-BuOH	2/3	120	7	Amorphous
MPTz	TAPP	6 M AcOH	*o*-DCB/*n*-BuOH	1/1	120	7	Crystalline
MPTz	TAPP	6 M AcOH	*o*-DCB/*n*-BuOH	3/2	120	7	Poorly crystalline
MPTz	TAPP	6 M AcOH	*o*-DCB/*n*-BuOH	7/3	120	7	Poorly crystalline
MPTz	TAPP	6 M AcOH	*o*-DCB/*n*-BuOH	4/1	120	7	Crystalline
MPTz	TAPP	6 M AcOH	*o*-DCB/*n*-BuOH	9/1	120	7	Crystalline
MPTz	TAPP	6 M AcOH	*o*-DCB	-	120	7	Amorphous
MPTz	TAPP	6 M AcOH	mesitylene	-	120	3	Crystalline
MPTz	TAPP	6 M AcOH	dioxane/mesitylene	1/9	120	3	Crystalline
MPTz	TAPP	6 M AcOH	dioxane/mesitylene	1/4	120	3	Crystalline
MPTz	TAPP	6 M AcOH	dioxane/mesitylene	3/7	120	3	Poorly crystalline
MPTz	TAPP	6 M AcOH	dioxane/mesitylene	2/3	120	3	Poorly crystalline
MPTz	TAPP	6 M AcOH	dioxane/mesitylene	1/1	120	3	Poorly crystalline
MPTz	TAPP	6 M AcOH	dioxane/mesitylene	3/2	120	3	Poorly crystalline
MPTz	TAPP	6 M AcOH	dioxane/mesitylene	7/3	120	3	Poorly crystalline
MPTz	TAPP	6 M AcOH	dioxane/mesitylene	4/1	120	3	Poorly crystalline
MPTz	TAPP	6 M AcOH	dioxane/mesitylene	9/1	120	3	Poorly crystalline
MPTz	TAPP	6 M AcOH	dioxane	-	120	3	Amorphous
MPTz	TAPP	6 M AcOH	mesitylene	-	120	7	Amorphous
MPTz	TAPP	6 M AcOH	dioxane/mesitylene	1/9	120	7	Crystalline
MPTz	TAPP	6 M AcOH	dioxane/mesitylene	1/4	120	7	Crystalline
MPTz	TAPP	6 M AcOH	dioxane/mesitylene	3/7	120	7	Amorphous
MPTz	TAPP	6 M AcOH	dioxane/mesitylene	2/3	120	7	Amorphous
MPTz	TAPP	6 M AcOH	dioxane/mesitylene	1/1	120	7	Amorphous
MPTz	TAPP	6 M AcOH	dioxane/mesitylene	3/2	120	7	Amorphous
MPTz	TAPP	6 M AcOH	dioxane/mesitylene	7/3	120	7	Amorphous
MPTz	TAPP	6 M AcOH	dioxane/mesitylene	4/1	120	7	Amorphous
MPTz	TAPP	6 M AcOH	dioxane/mesitylene	9/1	120	7	Amorphous
MPTz	TAPP	6 M AcOH	dioxane	-	120	7	Amorphous

Table S2. Peak assignments of FT-IR spectra for monomers, PTz-TPB-COF, PTz-BTA-COF, PTz-Py-COF, and OPTz-BTA-COF.

structure	peak (cm^{-1})	assignment
MPTz	2900 (w)	C-H asymmetric stretching vibration of CH_3 group
	2831 (w)	C-H symmetric stretching vibration of CH_3 group
	2810 (w), 2728 (w)	C-H stretching vibration of CHO group
	1679 (s)	C=O stretching vibration of CHO group
	1604 (m), 1570 (s), 1466 (s), 1414 (m)	skeleton vibration of benzene ring
	1437 (w)	C-H asymmetric deformation vibration of CH_3 group
	1376 (m)	C-H symmetric deformation vibration of CH_3 group
	1334 (s)	C-N asymmetric stretching vibration
	1259 (s)	C-N symmetrical stretching vibration
	1199 (s)	C-C stretching vibration between benzene ring and CHO group
	1104 (m)	C-S stretching vibration
	1132 (m), 1052 (w), 1011 (w)	C-H in-plane bending vibration of benzene ring
	894 (m), 818 (s)	C-H out-of-plane bending vibration of benzene ring
TAPB	3434 (m)	N-H asymmetric stretching vibration of NH_2 group
	3355 (s)	N-H symmetric stretching vibration of NH_2 group
	3209 (w)	overtone for deformation vibration of NH_2 group
	3053 (w), 3029 (w)	C-H stretching vibration of benzene ring
	1621 (s)	N-H deformation vibration of NH_2 group
	1607 (s), 1515 (s), 1448 (w), 1406 (w)	skeleton vibration of benzene ring
	1280 (s), 1241 (w)	C-N stretching vibration
	1128 (w), 1066 (w), 1012 (w)	C-H in-plane bending vibration of benzene ring
	872 (w), 829 (s), 707 (w)	C-H out-of-plane bending vibration of benzene ring
BTTA	3042 (w)	C-H stretching vibration of benzene ring
	2948 (m)	C-H asymmetric stretching vibration of CH_2 group
	2919 (m)	C-H symmetric stretching vibration of CH_2 group
	2252 (s)	C≡N stretching vibration of cyano group
	1609 (s), 1467 (s)	skeleton vibration of benzene ring
	1414 (s)	C-H deformation vibration of CH_2 group
	1287 (w), 1209 (w), 1166 (w)	C-H out-of-plane wagging vibration of CH_2 group
	830 (s), 686 (s)	C-H out-of-plane bending vibration of benzene ring
TAPP	3421 (w)	N-H asymmetric stretching vibration of NH_2 group
	3345 (m)	N-H symmetric stretching vibration of NH_2 group
	3216 (w)	overtone for deformation vibration of NH_2 group
	3055 (w), 3025 (w)	C-H stretching vibration of benzene ring
	1618 (s)	N-H deformation vibration of NH_2 group
	1608 (s), 1519 (s), 1494 (s),	skeleton vibration of benzene ring

	1458 (m), 1425 (w), 1382 (w)	
	1305 (m), 1279 (s)	C-N stretching vibration
	1126 (w), 1078 (w), 1003 (w)	C-H in-plane bending vibration of benzene ring
	834 (s)	C-H out-of-plane bending vibration of benzene ring
PTz-TPB-COF	3024 (w)	C-H stretching vibration of benzene ring
	2869 (w)	C-H stretching vibration of CH_3 group
	1683 (m)	C=N stretching vibration
	1593 (s), 1578 (s), 1504 (m), 1468 (s), 1397 (w)	skeleton vibration of benzene ring
	1334 (s), 1281 (m), 1259 (m)	C-N stretching vibration
	1105 (w)	C-S stretching vibration
PTz-BTA-COF	2211 (w)	C≡N stretching vibration of cyano group
	1668 (m)	C=C stretching vibration
	1594 (m), 1574 (s), 1472 (s), 1399 (w)	skeleton vibration of benzene ring
	1340 (m), 1264 (w)	C-N stretching vibration
	1109 (w)	C-S stretching vibration
PTz-Py-COF	3054 (w), 3025 (w)	C-H stretching vibration of benzene ring
	2882 (w), 2817 (w)	C-H stretching vibration of CH_3 group
	1684 (m)	C=N stretching vibration
	1599 (w), 1577 (m), 1547 (w), 1507 (w), 1469 (s), 1399 (m)	skeleton vibration of benzene ring
	1335 (s), 1281 (m), 1261 (m)	C-N stretching vibration
	1105 (w)	C-S stretching vibration
OPTz-BTA-COF	2214 (w)	C≡N stretching vibration of cyano group
	1669 (m)	C=C stretching vibration
	1591 (s), 1479 (s), 1415 (w)	skeleton vibration of benzene ring
	1347 (m)	C-N stretching vibration
	1291 (w)	O=S=O asymmetric stretching vibration
	1149 (w)	O=S=O symmetric stretching vibration

Table S3. Peak assignments of solid-state ^{13}C NMR spectra for PTz-TPB-COF, PTz-BTA-COF, PTz-Py-COF, and OPTz-BTA-COF.

structure	chemical shift (ppm)	assignment
PTz-TPB-COF	35	C of -CH_3 group
	115, 128, 131	other C of benzene ring
	141	C of benzene ring connecting another benzene ring
	148	C of benzene ring connecting N
	158	C of -CH=N group
PTz-BTA-COF	35	C of -CH_3 group
	106	C of -C(-R)= group
	109	C of -CN group
	115, 128, 135	other C of benzene ring
	143	C of benzene ring connecting N
	145	C of -CH= group
PTz-Py-COF	35	C of -CH_3 group
	115, 126, 132	other C of benzene ring
	136	C of benzene ring connecting pyrene
	147	C of benzene ring connecting N
	155	C of -CH=N group
OPTz-BTA-COF	36	C of -CH_3 group
	106	C of -C(-R)= group
	109	C of -CN group
	119, 128, 135	other C of benzene ring
	137	C of benzene ring connecting N
	140	C of -CH= group

Table S4. Elemental analysis results of PTz-TPB-COF, PTz-BTA-COF, PTz-Py-COF, and OPTz-BTA-COF.

COF		C%	H%	N%	S%
PTz-TPB-COF	Calcd.	79.63	4.53	8.99	6.86
	Found	77.85	3.34	9.02	7.11
PTz-BTA-COF	Calcd.	76.01	3.61	11.56	8.82
	Found	74.91	4.43	10.01	7.45
PTz-Py-COF	Calcd.	81.37	4.29	8.13	6.21
	Found	78.45	3.64	9.86	6.93
OPTz-BTA-COF	Calcd.	69.86	3.31	10.63	8.11
	Found	68.13	4.14	9.52	7.25

Table S5. Atomistic coordinates for the refined unit cell parameters for PTz-TPB-COF optimized via Pawley refinement (Space group: *P31M*; $a = b = 44.6434$ Å, $c = 3.7300$ Å; $\alpha = \beta = 90°$, $\gamma = 120°$).

Atom	*x/a*	*y/b*	*z/c*
C	0.70117	0.33963	0.48651
C	0.67284	0.30565	0.48735
C	0.73744	0.34621	0.47571
C	0.61250	0.23543	0.32740
C	0.58490	0.20166	0.30927
C	0.55179	0.19353	0.43595
C	0.57560	0.25401	0.60457
N	0.52235	0.16051	0.39372
H	0.63715	0.24069	0.21299
H	0.58880	0.18190	0.18083
C	0.03597	0.46720	0.24027
C	0.06801	0.49537	0.33430
C	0.09815	0.49262	0.34890
C	0.09459	0.46006	0.27572
H	0.33970	0.88282	0.28705
C	0.54765	0.22052	0.58020
C	0.52308	0.13200	0.42914
H	0.52251	0.21478	0.68381
H	0.57140	0.27368	0.72998
H	0.54668	0.13155	0.51973
C	0.56571	0.59802	0.16694
H	0.47979	0.54964	0.38919
C	0.43158	0.06252	0.19247
H	0.59299	0.65443	0.14682
H	0.67766	0.28405	0.48601
H	0.64002	0.61735	-0.24935
H	0.64306	0.64306	0.12871
C	0.62520	0.62520	-0.07833
S	0.47435	0.00000	0.19934
N	0.40512	0.00000	0.07286

Table S6. Atomistic coordinates for the AB-stacking mode of PTz-TPB-COF optimized by using DFTB+ method (Space group: *P31C*; $a = b = 43.5281$ Å, $c = 6.6567$ Å; $\alpha = \beta = 90°$, $\gamma = 120°$).

Atom	*x/a*	*y/b*	*z/c*
C	0.03517	1.00543	0.73554
C	0.00530	0.97098	0.73673
C	0.07200	1.01107	0.71999
C	-0.05681	0.89776	0.70878
C	-0.08542	0.86378	0.67623
C	-0.12013	0.85828	0.65159
C	-0.09610	0.92172	0.70398
N	-0.14873	0.82617	0.58223
H	-0.03066	0.90035	0.72213
H	-0.08042	0.84172	0.66051
C	-0.63166	1.12689	0.25746
C	-0.59572	1.15272	0.26431
C	-0.57119	1.15349	0.12215
C	-0.58392	1.12606	-0.02157
H	-0.30894	1.56577	-0.13132
C	-0.12480	0.88807	0.66865
C	-0.15429	0.79461	0.62204
H	-0.15129	0.88453	0.65321
H	-0.10153	0.94352	0.71405
H	-0.13869	0.78931	0.73583
C	-0.09969	1.25554	0.10898
H	-0.17340	1.23994	0.37856
C	-0.22517	0.74006	0.23795
H	-0.07873	1.29372	-0.13761
H	0.00944	0.94834	0.73530
H	-0.04597	1.23304	-0.12665
C	-0.32712	1.36848	-0.03721
C	-0.36199	1.33950	-0.03731
C	-0.32034	1.40594	-0.03443
C	-0.42968	1.26869	-0.19194
C	-0.46447	1.24034	-0.18915
C	-0.47707	1.21707	-0.02304
C	-0.41823	1.24948	0.12682
N	-0.51260	1.18857	-0.02475
H	-0.42065	1.28684	-0.31949
H	-0.48241	1.23680	-0.31248
C	-0.20683	0.70194	0.39878
C	-0.18493	0.72980	0.52756
C	-0.18128	0.76383	0.50799
C	-0.20291	0.76783	0.36482
H	0.20677	1.00489	0.35108
C	-0.45337	1.22179	0.13466
C	-0.53408	1.18279	0.12391

H	-0.46231	1.20358	0.26186
H	-0.40030	1.25273	0.24983
H	-0.52598	1.20069	0.25718
C	-0.06683	1.22622	0.24230
H	-0.10511	1.16950	0.64127
C	-0.61955	1.09959	-0.02580
H	-0.01383	1.24149	0.13224
H	-0.38429	1.34429	-0.03675
H	-0.06940	1.25273	-0.22348
H	-0.02881	1.27927	-0.09421
C	-0.05334	1.25318	-0.09599
S	-0.20877	0.66020	0.43720
N	-0.24509	0.68120	0.09198

Table S7. Atomistic coordinates for the refined unit cell parameters for PTz-BTA-COF optimized via Pawley refinement (Space group: *P31M*; $a = b = 30.3605$ Å, $c = 3.5701$ Å; $\alpha = \beta = 90°$, $\gamma = 120°$).

Atom	*x/a*	*y/b*	*z/c*
C	0.51142	0.14512	0.40457
C	0.46270	0.13912	0.35375
C	0.41910	0.09150	0.38280
C	0.42159	0.04742	0.47032
C	0.47073	0.05305	0.50541
C	0.51429	0.10061	0.46745
C	0.36496	0.80591	0.39232
C	0.32616	0.75874	0.48773
C	0.27827	0.75152	0.62535
C	0.33040	0.71183	0.47522
C	0.28594	0.66378	0.47552
N	0.74440	0.24037	0.75149
H	0.45823	0.17130	0.28042
H	0.38265	0.08914	0.33472
H	0.55137	0.10377	0.50242
H	0.40078	0.80868	0.30880
H	0.24927	0.66195	0.48047
H	0.69520	0.66173	0.77757
N	0.37650	0.00000	0.51999
S	0.47885	0.00000	0.61573
C	0.00000	0.32964	0.61360
H	0.69264	0.69264	0.37523

Table S8. Atomistic coordinates for the AB-stacking mode of PTz-BTA-COF optimized by using DFTB+ method (Space group: *P31C*; $a = b = 29.1861$ Å, $c = 7.1390$ Å; $\alpha = \beta = 90°$, $\gamma = 120°$).

Atom	*x/a*	*y/b*	*z/c*
C	0.82312	0.81597	0.11023
C	0.77279	0.81136	0.12781
C	0.72814	0.76316	0.17375
C	0.73089	0.71689	0.21254
C	0.78172	0.72176	0.19352
C	0.82566	0.76928	0.13944
C	0.67841	1.46811	0.32485
C	0.64472	1.42060	0.40784
C	0.59637	1.41061	0.49966
C	0.65635	1.37600	0.41102
C	0.61442	1.32320	0.41224
N	1.05124	0.87564	0.18424
H	0.76727	0.84494	0.10108
H	0.69058	0.76250	0.17832
H	0.86371	0.77103	0.12713
H	0.71452	1.47164	0.26508
H	0.57392	1.31573	0.41511
H	1.06278	1.35502	0.36732
C	0.48281	1.15909	0.30895
C	0.47810	1.10854	0.30891
C	0.42884	1.06258	0.29017
C	0.38081	1.06371	0.27684
C	0.38604	1.11496	0.27201
C	0.43545	1.16066	0.28437
C	1.13623	1.00981	0.07072
C	1.08347	0.97299	0.08560
C	1.06591	0.91870	0.13730
C	1.04111	0.98730	0.06705
C	0.98759	0.94711	0.06623
N	0.55821	1.40170	0.57878
H	0.51299	1.10428	0.31788
H	0.42872	1.02529	0.28458
H	0.43731	1.19888	0.28022
H	1.14542	1.04988	0.03518
H	0.97857	0.90616	0.07008
H	1.02849	1.38916	0.40134
N	0.68520	0.66892	0.26744
S	0.79426	0.66939	0.25115
C	0.32970	0.96597	0.30299
H	1.05191	1.38682	0.17476

Table S9. Atomistic coordinates for the refined unit cell parameters for PTz-Py-COF optimized via Pawley refinement (Space group: *CMM2*; a = 37.4096 Å, b = 23.3808 Å, c = 3.7389 Å; $\alpha = \beta = \gamma = 90°$).

Atom	*x/a*	*y/b*	*z/c*
C	0.48179	0.10493	0.84897
C	0.46134	0.05360	0.77403
C	0.42351	0.05367	0.71477
C	0.40238	0.10854	0.68020
C	0.41709	0.15840	0.51575
C	0.39888	0.21069	0.50371
C	0.36373	0.21517	0.63733
C	0.34783	0.16519	0.78865
C	0.36706	0.11346	0.81242
N	0.34746	0.72975	0.62073
C	0.26128	0.65842	0.44001
C	0.29840	0.66460	0.48151
C	0.31943	0.61395	0.46171
C	0.30404	0.56021	0.38930
C	0.26648	0.55400	0.34462
C	0.24548	0.60461	0.38065
C	0.31464	0.72224	0.52130
H	0.46845	0.14533	0.91499
H	0.44321	0.15654	0.38909
H	0.41121	0.24805	0.37565
H	0.32101	0.16723	0.90254
H	0.35453	0.07682	0.94821
H	0.24411	0.69627	0.45821
H	0.34827	0.61738	0.49090
H	0.21652	0.60298	0.36028
H	0.20912	0.46203	-0.04518
H	0.29736	0.75942	0.44290
C	0.48066	0.00000	0.77597
C	0.40612	0.00000	0.67673
H	0.37778	0.00000	0.60820
N	0.25026	0.50000	0.26477
C	0.21363	0.50000	0.12424
S	0.33368	0.50000	0.33274
H	0.19285	0.50000	0.33541

Table S10. Atomistic coordinates for the AB-stacking mode of PTz-Py-COF optimized by using DFTB+ method (Space group: *FMM2*; a = 36.4595 Å, b = 23.5469 Å, c = 7.0923 Å; $\alpha = \beta = \gamma = 90°$).

Atom	*x/a*	*y/b*	*z/c*
C	0.48126	0.60381	0.27609
C	0.46049	0.55273	0.24095
C	0.42156	0.55242	0.21648
C	0.40000	0.60654	0.20824
C	0.41108	0.65271	0.09400
C	0.39376	0.70526	0.10654
C	0.36304	0.71306	0.22529
C	0.35030	0.66585	0.33008
C	0.36872	0.61403	0.32297
N	0.34869	1.23145	0.24408
C	0.26335	1.15633	0.36879
C	0.30069	1.16371	0.32434
C	0.32230	1.11410	0.30195
C	0.30655	1.06000	0.30764
C	0.26804	1.05309	0.33465
C	0.24741	1.10264	0.37438
C	0.31525	1.22134	0.29786
H	0.46701	0.64340	0.30710
H	0.43397	0.64776	-0.00354
H	0.40394	0.74077	0.02342
H	0.32701	0.67017	0.42481
H	0.35937	0.57946	0.41357
H	0.24616	1.19322	0.39751
H	0.35163	1.11846	0.27634
H	0.21853	1.09968	0.41029
H	0.20163	0.96277	0.21207
H	0.29490	1.25603	0.32048
C	0.48021	0.50000	0.24153
C	0.40329	0.50000	0.20220
H	0.37376	0.50000	0.17674
N	0.25004	1.00000	0.32204
C	0.21008	1.00000	0.29304
S	0.33650	1.00000	0.27396
H	0.19438	1.00000	0.42571

Table S11. PLQY and lifetime of PTz-TPB-COF, PTz-BTA-COF, PTz-Py-COF, and OPTz-BTA-COF powders in air.

	λ_{em} (nm)	PLQY (%)	τ_1 (ns)	a_1	τ_2 (ns)	a_2	τ_3 (ns)	a_3	τ_{aver} (ns)
PTz-TPB-COF	582	1.1	1.19	5550.98	3.20	910.10	-	-	1.81
PTz-BTA-COF	660	6.7	1.18	535.87	2.59	508.95	-	-	2.13
PTz-Py-COF	566	1.4	1.06	5191.42	2.73	892.13	-	-	1.57
OPTz-BTA-COF	526	1.2	6.50×10^{-9}	4070.08	0.44	5159.69	1.90	440.23	0.83

Table S12. PLQY and lifetimes of PTz-TPB-COF, PTz-BTA-COF, PTz-Py-COF, and OPTz-BTA-COF dispersed in different organic solvents.

	solvents	λ_{em} (nm)	PLQY (%)	τ_1 (ns)	a_1	τ_2 (ns)	a_2	τ_3 (ns)	a_3	τ_{aver} (ns)
PTz-TPB-COF	**hexane**	488	1.0	4.72	374.56	9.40	4790.14	-	-	9.22
	tetrahydrofuran	526	15.6	0.93	5064.44	8.76	1265.04	-	-	6.41
	acetone	528	15.2	1.27	3550.42	8.13	2233.04	-	-	6.77
	dichloromethane	531	17.6	1.45	4250.55	10.05	1685.89	-	-	7.76
	acetonitrile	535	11.4	1.60	2890.76	8.29	2721.42	-	-	7.15
	methanol	569	2.9	0.88	4341.75	1.69	1969.91	-	-	1.26
PTz-BTA-COF	**hexane**	654	7.8	1.63	803.97	2.93	325.78	-	-	2.18
	tetrahydrofuran	650	6.3	1.35	833.15	2.81	346.30	-	-	2.03
	acetone	648	6.6	1.30	1397.04	2.65	592.56	-	-	1.93
	dichloromethane	650	6.8	1.03	547.15	2.46	487.20	-	-	2.00
	acetonitrile	648	5.9	1.40	986.81	3.18	205.71	-		1.97
	methanol	653	5.8	1.40	946.37	3.12	183.93	-	-	1.92
PTz-Py-COF	**hexane**	491	0.3	3.97	127.88	9.32	5098.79	-	-	9.26
	tetrahydrofuran	510	11.2	0.63	2941.44	1.97	2258.54	8.49	932.07	5.43
	acetone	526	5.9	1.39×10^{-3}	3747.05	0.48	4236.35	8.44	2014.60	7.58
	dichloromethane	530	14.1	0.59	3152.61	2.14	1536.17	10.64	1481.76	8.41
	acetonitrile	537	4.4	4.96×10^{-4}	3455.58	0.57	5368.37	8.07	1174.05	6.25
	methanol	484	3.9	2.89	5629.68	-	-	-	-	2.89
OPTz-BTA-COF	**hexane**	514	3.5	0.37	5547.77	1.26	383.36	5.30	31.01	0.83
	tetrahydrofuran	510	7.7	0.43	5034.11	1.24	790.07	4.56	56.82	0.98
	acetone	509	6.9	0.48	4810.16	1.35	837.68	3.81	106.87	1.09
	dichloromethane	508	5.2	0.45	5633.86	1.38	591.64	5.29	55.60	1.05
	acetonitrile	510	3.8	0.38	4850.80	1.02	760.01	3.00	100.38	0.82
	methanol	504	4.6	0.02	3952.06	0.42	4538.06	1.73	395.91	0.75

Table S13. Polymerization performance metrics of the reported photocatalytic materials.

No	Photocatalyst (PC)	[M]:[initiator]:[PC] (mol%)	Light	Time (hour)	Conversion (%)	Mw (kDa)	Đ (Mw/Mn)	ref.
1	eosin Y	[MMA]:[CPADB]:[PC] 10000:0:1	Blue LEDs	24	5.0	950.0	3.80	S8
2	TTT–BTDA-COF	[MMA]:[TEA] 9.39:0.35	420–700 nm	12	54.0	710.4	2.92	S9
3	**OPTz-BTA-COF**	**[MMA]:[EBP]:[PC] 1000:10:1**	**Xe lamp**	**9**	**29.0**	**471.1**	**1.56**	**This work**
4	perylene	[MMA]:[EBP]:[PC] 875000:9000:1	White LEDs	24	28.3	429.0	1.57	S10
5	TX-CMP	[MMA]:[TEA] 3.13:0.023	Visible light	4	15.0	343.4	1.70	S11
6	$RbTe_{1.5}W_{0.5}O_6$	[water]:[MMA]:[pectin] 70:25:5	White LEDs	5	10.0	315.0	2.20	S12
7	FL	[MMA]:[EBPA]:[PC]:[Et_3N] 1000:5:1:30	Yellow LEDs	22	18.6	281.0	1.57	S13
8	P25 TiO_2	1.0 g L^{-1}	365 nm	5	84.4	234.0	2.70	S14
9	mpg-C_3N_4	[MMA]:[N,N-dimethylaniline] 9.35:0.256	> 420 nm	2	10.0	216.6	2.38	S15
10	PhPTZ	[MMA]:[BiBSiOEt]:[PC] 5000:10:1	365 nm	1	6.4	213.9	1.91	S16
11	TT-TPE	[MMA]:[EBI]:[PC] 800:2:1	~ 350 nm	16	6.1	201.8	1.68	S17
12	nano-TiO_2	Adding hole scavenger	365 nm	5	35.1	171.4	3.28	S18
13	dimethyl-dihydroacridine-3	[BA]:[DBMM]:[PC] 1000:10:1	365 nm	1	42.0	154.8	4.93	S19
14	pyrene	[t-BA]:[EBP]:[PC] 100:0.25:1	~ 350 nm	0.67	52.2	141.2	1.32	S20
15	TIPS-AN	[MMA]:[EBP]:[PC] 1000:10:1	365 nm	4	29.0	132.0	2.56	S21
16	5,10-diphenyl-5,10-dihydrophenazines-3	[MMA]:[EBP]:[PC] 1000:2:1	White LEDs	8	95.2	85.5	1.54	S22
17	Ph-benzoPTZ	[MMA]:[EBiB]:[PC] 1000:10:1	392 nm	24	78.0	73.3	1.60	S23
18	structure of N,Ndiaryl dihydrophenazine	[MMA]:[DBMM]:[PC] 10000:10:1	White LEDs	8	63.5	62.8	1.36	S24
19	MOF-901	[MMA]:[EBP]:[PC] 100:0.61:0.034	Visible light	18	87.0	43.0	1.60	S25
20	PTZ-CMP, $CuBr_2$	[MA]:[EBiB]:[$CuBr_2$]:[PMDETA] 1000:10:1	Green LEDs	4	94.0	41.6	2.06	S26

Supporting References

S1. http://www.dftb.org.

S2. Aradi, B.; Hourahine, B.; Frauenheim, T. DFTB+, a Sparse Matrix-Based Implementation of the DFTB Method. *J. Phys. Chem. A* **2007**, *111*, 5678.

S3. Gaus, M.; Goez, A.; Elstner, M. Parametrization and Benchmark of DFTB3 for Organic Molecules. *J. Chem. Theory Comput.* **2013,** *9*, 338.

S4. Gaus, M.; Lu, X.; Elstner, M.; Cui, Q. Parameterization of DFTB3/3OB for Sulfur and Phosphorus for Chemical and Biological Applications. *J. Chem. Theory Comput.* **2014,** *10*, 1518.

S5. Kubillus, M.; Kubar, T.; Gaus, M.; Rezac, J.; Elstner, M. Parameterization of the DFTB3 Method for Br, Ca, Cl, F, I, K, and Na in Organic and Biological Systems. *J. Chem. Theory Comput.* **2015,** *11*, 332.

S6. Lu, X.; Gaus, M.; Elstner, M.; Cui, Q. Parametrization of DFTB3/3OB for Magnesium and Zinc for Chemical and Biological Applications. *J. Phys. Chem. B* **2015,** *119*, 1062.

S7. Berar, J.-F.; Baldinozzi, G. Modeling of Line-Shape Asymmetry in Powder Diffraction. *J. Appl. Crystallogr.* **1993**, *26*, 128.

S8. Xu, J.; Shanmugam, S.; Duong, H. T.; Boyer, C. Organo-Photocatalysts for Photoinduced Electron Transfer-Reversible Addition–Fragmentation Chain Transfer (PET-RAFT) Polymerization. *Polym. Chem.* **2015**, *6*, 5615.

S9. Pachfule, P.; Acharjya, A.; Roeser, J.; Sivasankaran, R. P.; Ye, M.-Y.; Bruckner, A.; Schmidt, J.; Thomas, A. Donor–Acceptor Covalent Organic Frameworks for Visible Light Induced Free Radical Polymerization. *Chem. Sci.* **2019**, *10*, 8316.

S10. Miyake, G. M.; Theriot, J. C. Perylene as an Organic Photocatalyst for the Radical Polymerization of Functionalized Vinyl Monomers through Oxidative Quenching with Alkyl Bromides and Visible Light. *Macromolecules* **2014**, *47*, 8255.

S11. Dadashi-Silab, S.; Bildirir, H.; Dawson, R.; Thomas, A.; Yagci, Y. Microporous Thioxanthone Polymers as Heterogeneous Photoinitiators for Visible Light Induced Free Radical and Cationic Polymerizations. *Macromolecules* **2014**, *47*, 4607.

S12. Semenycheva, L; Chasova, V.; Matkivskaya, J.; Fukina, D.; Koryagin, A.; Belaya, T.; Grigoreva, A.; Kursky, Y.; Suleimanov, E. Features of Polymerization of Methyl Methacrylate using a Photocatalyst—the Complex Oxide $RbTe_{1.5}W_{0.5}O_6$. *J. Inorg. and Organomet. P.* **2021**, *31*, 3572.

S13. Liu, X.; Zhang, L.; Cheng, Z.; Zhu, X. Metal-free Photoinduced Electron Transfer–Atom Transfer Radical Polymerization (PET–ATRP) via a Visible Light Organic

Photocatalyst. *Polym. Chem.* **2016**, *7*, 689.

S14. Dong, C.; Ni, X. The Photopolymerization and Characterization of Methyl Methacrylate Initiated by Nanosized Titanium Dioxide. *J. Macromol. Sci. A* **2004**, *41*, 547.

S15. Kiskan, B.; Zhang, J.; Wang, X.; Antonietti, M.; Yagci, Y. Mesoporous Graphitic Carbon Nitride as a Heterogeneous Visible Light Photoinitiator for Radical Polymerization. *ACS Macro Lett.* **2012**, *1*, 546.

S16. Yan, J.; Pan, X.; Schmitt, M.; Wang, Z.; Bockstaller, M. R.; Matyjaszewski, K. Enhancing Initiation Efficiency in Metal-Free Surface-Initiated Atom Transfer Radical Polymerization (SI-ATRP). *ACS Macro Lett.* **2016**, *5*, 661.

S17. Kutahya, C.; Allushi, A.; Isci, R.; Kreutzer, J.; Ozturk, T.; Yilmaz, G.; Yagci, Y. Photoinduced Metal-Free Atom Transfer Radical Polymerization Using Highly Conjugated Thienothiophene Derivatives. *Macromolecules* **2017**, *50*, 6903.

S18. Ye, J.; Ni, X.; Dong, C. Electric Charge Scavenger Effects in PMMA Photopolymerization Initiated by TiO_2 Semiconductor Nanoparticles. *J. Macromol. Sci. A* **2005**, *42*, 1451.

S19. Buss, B. L.; Lim, C.-H.; Miyake, G. M. Dimethyl Dihydroacridines as Photocatalysts in Organocatalyzed Atom Transfer Radical Polymerization of Acrylate Monomers. *Angew. Chem. Int. Ed.* **2020**, *59*, 3209.

S20. Allushi, A.; Jockusch, S.; Yilmaz, G.; Yagci, Y. Photoinitiated Metal-Free Controlled/Living Radical Polymerization Using Polynuclear Aromatic Hydrocarbons. *Macromolecules* **2016**, *49*, 7785.

S21. Pan, X.; Fang, C.; Fantin, M.; Malhotra, N.; So, W. Y.; Peteanu, L. A.; Isse, A. A.; Gennaro, A.; Liu, P.; Matyjaszewski, K. Mechanism of Photoinduced Metal-Free Atom Transfer Radical Polymerization: Experimental and Computational Studies. *J. Am. Chem. Soc.* **2016**, *138*, 2411.

S22. Theriot, J. C.; Lim, C.-H.; Yang, H.; Ryan, M. D.; Musgrave, C. B.; Miyake, G. M. Organocatalyzed Atom Transfer Radical Polymerization Driven by Visible Light. *Science* **2016**, *352*, 1082.

S23. Dadashi-Silab, S.; Pan, X.; Matyjaszewski, K. Phenyl Benzo[*b*]phenothiazine as a Visible Light Photoredox Catalyst for Metal-Free Atom Transfer Radical Polymerization. *Chem. Eur. J.* **2017**, *23*, 5972.

S24. Cole, J. P.; Federico, C. R.; Lim, C.-H.; Miyake, G. M. Photoinduced Organocatalyzed Atom Transfer Radical Polymerization Using Low ppm Catalyst Loading. *Macromolecules* **2019**, *52*, 747.

S25. Nguyen, H. L.; Gándara, F.; Furukawa, H.; Doan, T. L. H.; Cordova, K. E.; Yaghi, O. M. A Titanium−Organic Framework as an Exemplar of Combining the Chemistry of Metal− and Covalent−Organic Frameworks. *J. Am. Chem. Soc.* **2016**, *138*, 4330.

S26. Dadashi-Silab, S.; Lorandi, F.; DiTucci, M. J.; Sun, M.; Szczepaniak, G.; Liu, T.; Matyjaszewski, K. Conjugated Cross-linked Phenothiazines as Green or Red Light Heterogeneous Photocatalysts for Copper-Catalyzed Atom Transfer Radical Polymerization. *J. Am. Chem. Soc.* **2021**, *143*, 9630.